https://doi.org/10.5194/egusphere-2026-5038
Preprint. Discussion started: 25 August 2026

Biogeochemical and microbial microseepage connectivity from a deeply buried salt diapir on the Scotian Slope of Atlantic Canada

Gamra Oueslati[1*], Elish Redshaw[1], Unyime U. Umoh[1], Natasha MacAdam[2], Patricia Granados[3], Jeremy N. Bentley[1], Robbie Bennett[4], Venus Baghalabadi[1,5], Adam MacDonald[2], Calvin Campbell[4], Martin G. Fowler[6], and G. Todd Ventura[1*]

[1]Department of Geology, Saint Mary's University, 923 Robie Street, Halifax, Nova Scotia B3H 3C3, Canada
[2]Nova Scotia Department of Energy, 1690 Hollis St., Halifax, Nova Scotia B3J 3J9, Canada
[3]Centre for Environmental Analysis and Remediation, Saint Mary's University, 923 Robie Street, Halifax, Nova Scotia B3H 3C3, Canada
[4] Natural Resources Canada, Geological Survey of Canada, 1 Challenger Drive, Dartmouth, Nova Scotia B2Y 4A2, Canada
[5]Department of Pharmacology, Dalhousie University, 5850 College St, Halifax, Nova Scotia, B3H 4R2, Canada
[6]Applied Petroleum Technology (Canada) Ltd., Calgary, AB T3A 2M3, Canada

Correspondence to: Gamra Oueslati (Gamra.Oueslati@smu.ca) and G. Todd Ventura (todd.ventura@smu.ca)

Keywords: cold seep, Archaea, porewater, methane, AMNE, biomarker, Scotian Slope, salt diapir

Abstract:

Cold seeps are seafloor environments where hydrocarbon-rich fluids, including methane and hydrogen sulfide, migrate through deep-seated faults and fractures to the seabed, supporting chemosynthetic communities. Although the biological activity within and immediately around these sites can be highly elevated compared to the surrounding deep-ocean ambient sediments, little is known about whether subtle changes extend to the larger periphery, where no visible signs of seepage exist. Here we examine how geological structures, such as subsurface faults, regulate seep formation and fluid migration, and assess the influence this has on microbial distributions by combining a 2.5×2.5×1 km three-dimensional seismic survey with a 1.6 km transect study that overlies a deeply buried salt diapir. The crest of the diapir rests ~1 km below the seafloor, where it has heavily disturbed the overlying bedrock with radial and crustal faults, half-graben block displacements, and salt-tectonic-influenced anticlinal mini-basins. Rocks draping the diapir also host a subsurface methanogenic deep biosphere that produces sufficient methane to sustain a biodiverse ocean floor cold seep. A portion of the produced hydrocarbons has become trapped within ~300 mbsf block-faulted strata where they are recognizable in seismic data as a direct hydrocarbon indicator (DHI). We analyzed 52 sediment samples extending 5–575 cm below seafloor (cmbsf) from five gravity cores and one push core collected at an active cold seep. Spatial heterogeneity in cored sediments along the transect was revealed by porewater geochemistry, stable isotopes, and lipidomics. Collectively, these data resolve distinct chemosynthetic zones that form tightly coupled functional networks mediated by interlinked redox-dependent cycling of nitrogen, carbon, iron, and manganese that are comprised of ammonia-oxidizing archaea (AOA), anaerobic methanotrophs (ANMEs), and sulfate-reducing bacteria (SRB). Evidence is provided that microbial assemblages and their metabolic interactions are shaped and sustained by diffuse and largely non-detectable microseepage ascending along more deeply buried fault systems associated with the salt diapir. The results, therefore, establish a spatially resolved model for offshore geochemical surveys that link subsurface fluid flow to redox gradients and microbial activity.

https://doi.org/10.5194/egusphere-2026-5038
Preprint. Discussion started: 25 August 2026

1. Introduction

Cold seeps occur along both passive and active continental margins, where the upward migration of reduced fluids from deep subsurface reservoirs through faults and fractures (Suess, 2014; Joye et al., 2020) supports substantial chemosynthetic biomass (Levin, 2005; Foucher et al., 2009). These fluids also transport heavy hydrocarbon gases, brines, and waters (Judd and Hovland, 2007; Suess, 2014), with their composition and discharge rates influenced by subsurface geology, which in turn regulates the availability of energy for microbial metabolism (Levin et al., 2005; Jørgensen and Boetius, 2007; Foucher et al., 2009; Suess, 2014; Joye, 2020). Anaerobic oxidation of methane (AOM) is a key microbial process in cold seeps, mediated by syntrophic consortia of methanotrophic archaea (ANME) and sulfate-reducing deltaproteobacteria (SRB). The distribution of ANME is linked to methane availability, sediment geochemistry, and habitat conditions (Ruff et al., 2015), while localized variations in fluid advection create steep geochemical gradients that further drive microbial zonation over spatial scales (Levin, 2005). AOM typically occurs within the narrow sediment interval known as the sulfate-methane transition zone (SMTZ), where it consumes upward-migrating CH_4 and converts it to bicarbonate (HCO_3^-), thereby acting as a major biological sink for methane in marine sediments (Boetius et al., 2000; Knittel et al., 2005; Knittel and Boetius, 2009). As a result, AOM increases alkalinity in marine porewaters and facilitates authigenic carbonate precipitation near the seafloor (Eq. 1; Hinrichs et al., 1999; Treude et al., 2005; Meister et al., 2018). Methane oxidation can also be mediated by alternative electron acceptors, such as nitrate (Haroon et al., 2013; NO_3^-), nitrite (Ettwig et al., 2010; NO_2^-), and metal oxides (Ettwig et al., 2016; Beal et al., 2009; Eq. 3, 4), in addition to sulfate (SO_4^{2-}).

$$CH_4 + SO_4^{2-} \rightarrow HCO_3^- + HS^- + H_2O \quad (1)$$

The co-occurrence of methanotrophs, sulfate-reducing bacteria, and nitrogen-cycling microorganisms in cold seep sediments indicates tightly coupled methane, sulfur, and nitrogen cycling that sustains seep ecosystems (Wang et al., 2025). However, the mechanisms by which geological heterogeneity generate chemical gradients that structure microbial niches and drive taxonomic and functional variation within cold seeps remain poorly understood. The Scotian Slope, represents a major segment of the Nova Scotian continental margin that transitions into deep ocean water that records over 250 million years of subsidence and sediment accumulation, with hydrocarbon reservoir potential strongly influenced by salt-related deformation and sediment instability (Sherwin, 1973). Basin evolution has produced an extensive salt-tectonic system characterized by distinct diapir- and canopy-dominated provinces (Albertz et al., 2010; Deptuck et al., 2017; Supplementary Fig. S3). Within this system, the Shelburne Subbasin constitutes a southwestern subdivision of the Scotian Basin, spanning ~ 100,000 km² (Wade and MacLean, 1990; Supplementary Fig. S1). Its extensive salt structures are associated with seismic amplitude anomalies, including direct hydrocarbon indicators (DHIs) that reside directly above diapirs, suggesting hydrocarbon-bearing sediments (Supplementary Figs. S1, S2). Cold seeps also occur around these salt diapirs (Campbell, 2019; Supplementary Fig. S3). The region therefore offers an ideal setting to address existing knowledge gaps pertaining to deeper basin geological structural influence of fluid flow on relatively shallow sediment hosted microbial ecosystem.

Diverse microbial assemblages have been documented in both shallow and deeply buried sediments associated with these locations (Dong et al., 2020; Li et al., 2023; Ahangarian et al., 2026). Surrounding benthic sediments support complex communities that are strongly influenced by hydrocarbon seepage and vary substantially with depth, exhibiting a pronounced stratification that reflects the dynamic conditions of hydrocarbon-rich environments (Gittins et al., 2022; Li et al., 2023). This aligns with documented changes in microbial distribution, particularly at boundaries of strong geochemical gradients (Redshaw et al., 2026), raising the question of how salt-related subsurface structure and associated geochemical gradients influence microbial community composition and function. Cold seep 2A-1, situated ~400 km offshore southeastern Nova Scotia, represents a geologically complex system where salt tectonism

https://doi.org/10.5194/egusphere-2026-5038
Preprint. Discussion started: 25 August 2026

governs subsurface architecture and fluid migration (Campbell and Normandeau, 2020). The seep primarily emits biogenic methane through the carbonate-hosted depression referred to as "The Hole." Gas hydrates are present beneath authigenic carbonate blocks that support chemosynthetic communities (Campbell and Normandeau, 2019; Bennett and Desiage, 2022; Chowdhury et al., 2024; Redshaw et al., 2026; Supplementary Fig. S4).

This study hypothesizes that the structural configuration of buried salt diapirs controls fluid migration pathways, thereby creating spatially heterogeneous geochemical gradients that structure microbial communities and drive subsurface carbon mobilization beyond the immediate active seep site. It further investigates whether spatial patterns in microbial distribution correspond to these geochemical gradients and align with fluid transport along pathways associated with the underlying salt structures. Addressing this hypothesis requires molecular proxies capable of resolving microbial responses across geochemical gradients. Lipid analyses reveal the structural diversity and functional characteristics of microbial consortia, offering insight into biogeochemical processes associated with seep (Van Mooy and Fredricks, 2010; Chevalier et al., 2014; Redshaw et al., 2026) and ambient deep marine environments (Ahangarian et al., 2026). Here, membrane lipids, including core lipids (CLs) and intact polar lipids (IPLs), which consist of hydrophobic core structures linked to hydrophilic headgroups, are characterized to assess microbial community variability. Additionally, menaquinone respiratory pigments (MKs) are analyzed to constrain microbial community composition and metabolic activity (Urakawa et al., 2005; Elling et al., 2016; Becker et al., 2018). Lipid distributions are interpreted alongside porewater chemistry, bulk geochemistry, and geophysical observations to identify the environmental controls governing microbial variability within the Scotian Slope seep system.

https://doi.org/10.5194/egusphere-2026-5038
Preprint. Discussion started: 25 August 2026

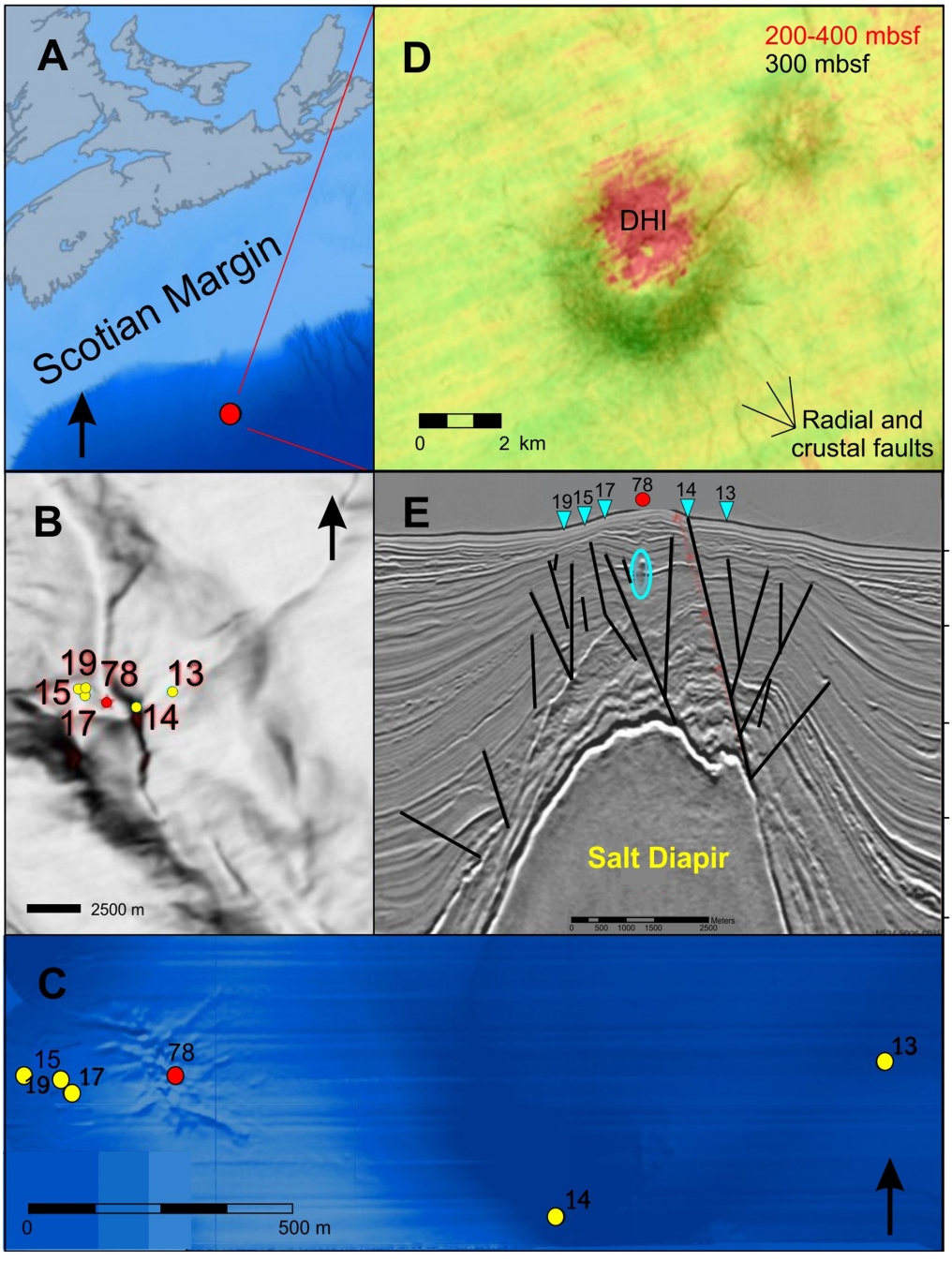

Figure 1. Seismic and bathymetric overview of the study area. A) Map of the Scotian Slope near the southern coast of Nova Scotia, Canada indicating the location of seep site 2A-1. B) Seismic coherence map showing the main fault zone and pockmark features. C) High-resolution bathymetric map illustrating the spatial distribution of sediment cores within a seafloor valley (NSDoE, 2025). D) 3D seismic RMS

https://doi.org/10.5194/egusphere-2026-5038
Preprint. Discussion started: 25 August 2026

map showing the location of the DHI (red area). RMS was calculated with a ±100 m integration window (red font) at a 300 mbsf target depth (black font). The structural alteration of the rock strata overlying a more deeply buried salt diapir is indicated by the dark green color that marks anticlinal strata bisected by radial and crustal faults. E) Strike-oriented seismic profile displaying velocity pull-ups and amplitude dimming indicative of gas-charged sediments (light blue ellipse), and diapiric faulting that suggests pathways for deep fluid migration (Shell Canada Ltd. via NSDoE).

2. Materials and methods

2.1. Sample collection

Cold seep site 2A-1 (42.162698/-62.372356), located at 2687 mbsl (m below sea level) along the Scotian Slope of the North Atlantic Ocean, was first identified in 2018 from an Autonomous Underwater Vehicle (AUV) survey over a large, buried salt diapir (Campbell and Normandeau 2019). Seep site 2A-1 was subsequently selected for Remotely Operated Vehicle (ROV) investigation (Bennet and Desiage 2022). Samples were collected along a 1.6-km transect spanning a gradient of seep influence, with five gravity cores (15, 19, 17, 14, and 13) and one seep-sourced push core (78, The Hole) (Supplementary Table S1), yielding 52 samples. Cores 15, 19, and 17 located near the seep, and cores 14 and 13 positioned 515 m and 1.26 km away, respectively (Fig. 1; Supplementary Fig. S3). Gravity cores were collected during the 2018 Scotian Slope expedition using the CCGS Hudson (Campbell and Normandeau 2019), which also surveyed the seep structure with an autonomous underwater vehicle (AUV) equipped with multibeam sonar. Samples from The Hole were collected in 2021 aboard the Atlantic Condor using a push coring system designed by the OGL group at Saint Mary's University (Bennett and Desiage 2022). Each core barrel was 50 cm in length, had an internal diameter of 8.89 cm, and penetrated to a depth of 38 cmbsf. An ROV equipped with advanced sensors was deployed during the 2021 expedition. After retrieval, the cores were sectioned into 2–4 cm intervals. Each subsample was wrapped in pre-baked aluminum foil and stored at -80 °C to preserve sample integrity prior to analysis.

2.2. Headspace gas analyses

Sediment from the lowermost 20 cm of each core was transferred to 500 mL IsoJars (Isotech Laboratories, Inc.), flushed with nitrogen, sealed, and stored at -20 °C until analysis. Cores selected based on DHIs underwent analysis for headspace gas composition, carbon isotopes, biomarkers, and sediment extract composition using gas chromatography-mass spectrometry (GC-MS). The resulting data enabled characterization of hydrocarbon composition and assessment of biogenic and thermogenic sources (Supplementary Table S1). Geochemical analyses were conducted by Dr. Martin Fowler at Applied Petroleum Technology AS.

2.3. Bulk geochemical analyses

The total organic carbon (TOC) content of sediment samples was quantified using a modified version of Kahn's (1988) method. Approximately 2.5 g of frozen sediment was dried at 35 °C for at least 12 hrs. After drying, samples were treated with 5 mL of 6N hydrochloric acid (HCl) and allowed to decarbonate for 24 hrs. Acid-treated samples were neutralized by repeated washing with deionized water until a pH of 7 was achieved. Neutralized samples were dried again at 35 °C for 12 hrs and subsequently stored at 4 °C until analysis. TOC concentrations were measured using a Perkin-Elmer 2400 Series II CHNS/O Elemental Analyzer (EA) configured for CHN analysis. All analyses were conducted at the Centre for Environmental Analysis and Remediation, Saint Mary's University. Four decarbonated sediment samples from each core were selected for bulk organic stable carbon isotope analysis ($\delta^{13}C_{org}$). Samples were analyzed by the Isotope Science Laboratory (ISL) at the University of Calgary, Canada. Carbon isotope ratios ($^{13}C/^{12}C$) were measured using Continuous Flow Elemental Analysis-Isotope Ratio Mass Spectrometry (CF-EA-IRMS) coupled with an Elementar Isotope CUBE® elemental analyzer. The

https://doi.org/10.5194/egusphere-2026-5038
Preprint. Discussion started: 25 August 2026

isotope ratios were presented in delta (δ) notation, which expresses the per mil (‰) deviation of the ratio relative to the Vienna Peedee Belemnite (VPDB) standard (Eq. 2; Craig, 1957).

$$\delta^{13}C = \left[\frac{\left({}^{13C}/_{12C}\right)_{Sample}}{\left({}^{13C}/_{12C}\right)_{Std}} - 1\right] \times 1000 \quad (2)$$

2.4. Porewater chemistry

Porewater analyses were performed at the Organic Geochemistry Laboratory, Saint Mary's University. Approximately 40 g of frozen sediment was placed in pre-cleaned polycarbonate centrifuge tubes, defrosted for up to 2 h, and centrifuged at 2500 rpm for 10 min. The extracted porewater was collected, filtered through 0.45-µm filters to remove suspended particles, and the recovered volume was recorded to estimate sediment porosity. Alternating sediment intervals of approximately 4 cm were designated for anion and cation analyses, except for the 0–2 cm surface interval, which was analyzed for both. Anion concentrations, including fluoride (F^-), NO_2^-, NO_3^-, SO_4^{2-}, and dissolved inorganic carbon (DIC; the combined signal of HCO_3^- and carbonate (CO_3^{2-}), were determined by ion chromatography using a Thermo Scientific Dionex Aquion Chromatography Conductivity System. Filtered porewater was diluted with high pressure liquid chromatographic (HPLC)-grade water prior to analysis; data acquisition and instrument control were managed using Chromeleon 7 software (version 7.3, Thermo Scientific). The concentrations were quantified using external calibration curves prepared from standard solutions. Cation and nutrient concentrations, including ammonium (NH_4^+), iron (II) (Fe^{2+}), manganese (II) (Mn^{2+}), and phosphate (PO_4^{3-}), were measured using a Hanna Instruments HI-83300 Multiparameter Photometer. Samples were diluted with Milli-Q water or appropriate reagents and corrected for dilution factors after measurement. Analyses of Fe^{2+}, Mn^{2+}, and PO_4^{3-} were conducted only for samples with sufficient porewater recovery to ensure reliable quantification. Data acquisition and instrument control were managed using Chromeleon 7 software (version 7.3, Thermo Scientific).

2.5. Lipid extraction and analysis

Lipids were extracted following a modified Bligh and Dyer protocol (Bligh and Dyer, 1959; Sturt et al., 2004; Bentley et al., 2022). Frozen samples were spiked with a recovery standard, 1-alkyl-2-acetyl-sn-glycerol-3-phosphocholine (PAF; Avanti Polar Lipids, Inc.). Three organic solvent mixtures were prepared: methanol, dichloromethane (as a substitute for chloroform), and phosphate buffer in a 2:1:0.8 volume ratio; methanol, dichloromethane, and trichloroacetic acid buffer in the same ratio; and methanol with dichloromethane in a 5:1 volume ratio. For each extraction, 3 mL of each mixture was added twice. The sediment-solvent mixture was sonicated and centrifuged at 1250 rpm for 5 min. Combined extracts were transferred to separation funnels and purified with Milli-Q water. The purified extract was evaporated under a stream of dry nitrogen and heated to 40 °C. The total lipid extract (TLE) was spiked with 1,2-diheneicosanoyl-sn-glycero-3-phosphocholine (C21-PC; Avanti Polar Lipids) and stored at -20 °C until mass spectral analysis.

An aliquot corresponding to 1% of the TLE was analyzed using an Agilent 1260 Infinity ultra- high performance- liquid chromatographic (UHPLC) system coupled to an Agilent Technologies 6530 quadrupole time-of-flight mass spectrometer (qTOF-MS) with electrospray ionization (ESI). Lipids were separated according to hydrophobic characteristics using a reverse-phase (RP) column (ZORBAX RRHD Eclipse Plus C18). Lipids were identified by their $[M + H]^+$, $[M + Na]^+$, and $[M + NH_4]^+$ pseudo-molecular ions and were tentatively characterized using retention times, molecular masses, and fragmentation patterns. Lipid detection was performed using Agilent Technologies MassHunter 10.0 software and in accordance with previous studies (Yoshinaga et al., 2011; Wörmer et al., 2015). Individual lipid concentrations were quantified relative to the internal standard C21-PC (Eq. 3) and expressed as µg per gram of sediment (µg·g sed^{-1}).

https://doi.org/10.5194/egusphere-2026-5038
Preprint. Discussion started: 25 August 2026

$$[Lipid] = \left(\frac{Mass_{Std} \times Area_{Lipid}}{Area_{Std} \times Mass_{Lipid}}\right) \times Dilution\ \% \quad (3)$$

2.6. Statistical analysis

Statistical analyses of lipid and porewater chemistry datasets were performed using RStudio (version 4.4.2). Hierarchical clustering analysis (HCA) was applied to z-scored lipid data (Eq. 4) using the "Stats" package and performed using Ward's minimum-variance method and Euclidean distance. Principal component analysis (PCA) was performed using the "FactoMineR" and "FactoExtra" packages. Data visualization was achieved using the "ggplot2" package.

$$z = \left(\frac{x - \bar{x}}{S}\right) \quad (4)$$

where x is the measured concentration of the lipid in each sample, $\bar{x}$ is the mean lipid concentration across all samples, and S denotes the sample standard deviation.

3. Results

3.1. Gas seepage and bulk organic matter patterns

Site 78 collected within a carbonate crag termed 'The Hole' with active biogenic methane seepage contained gas hydrates. However, no evidence of gas hydrates was observed in the recovered gravity cores. Core 15 exhibited the highest methane concentrations, consistent with a predominantly biogenic methane source. Apart from minor thermogenic input detected in core 14, the gas and biomarker data provide no evidence for substantial thermogenic hydrocarbon contributions or active petroleum seepage in the study area (Fowler and Webb, 2018). As such, all gravity cores were determined to be largely hydrocarbon negative and indicative of slope ambient sediment conditions.

Total organic carbon (TOC), total nitrogen (TN), carbon-to-nitrogen ratios (C/N), and $\delta^{13}C_{org}$ were measured in all sediment cores (Fig. 2; Supplementary Table S3). The resulting TOC profiles revealed three distinct stratigraphic patterns, indicating spatial heterogeneity. Cores 15, 19, and 17 exhibited low TOC concentrations, ranging from 0.24 to 0.69 wt.%. In contrast, cores 14 and 13 displayed moderately higher TOC values with minimal variability (0.29–0.74 wt.%). The Hole was characterized by a pronounced TOC maximum of 1.3 wt.% at 4 cmbsf followed by a marked decline of concentrations with depth, and TN distributions closely mirrored those of TOC, decreasing from 0.18 wt.% at the sediment-water interface (SWI) to 0.08 wt.% in deeper sediments. Downcore C/N ratios in cores 15, 19, and 17 ranged from 4 to 14, with a notable sharp peak of 30 in core 19 at 334 cmbsf. The Hole consistently exhibited low C/N values (mean 5.4). In cores 14 and 13, C/N ratios remained relatively stable in the upper ~300 cmbsf (5–10), with moderate fluctuations between 300 and 500 cmbsf, reaching a maximum of 15. These variations reflect changes in organic matter sources or input with depth. Values of $\delta^{13}C_{org}$ ranged from -25‰ to -21‰ in all cores, while The Hole displayed a pronounced gradient from -40‰ at the sediment surface to -26‰ at depth (Redshaw et al., 2026). Overall, the seep exhibited a distinct organic carbon signature in surface sediments compared to other transect cores, characterized by higher surface TOC and more depleted carbon isotope values (Fig. 2).

https://doi.org/10.5194/egusphere-2026-5038
Preprint. Discussion started: 25 August 2026

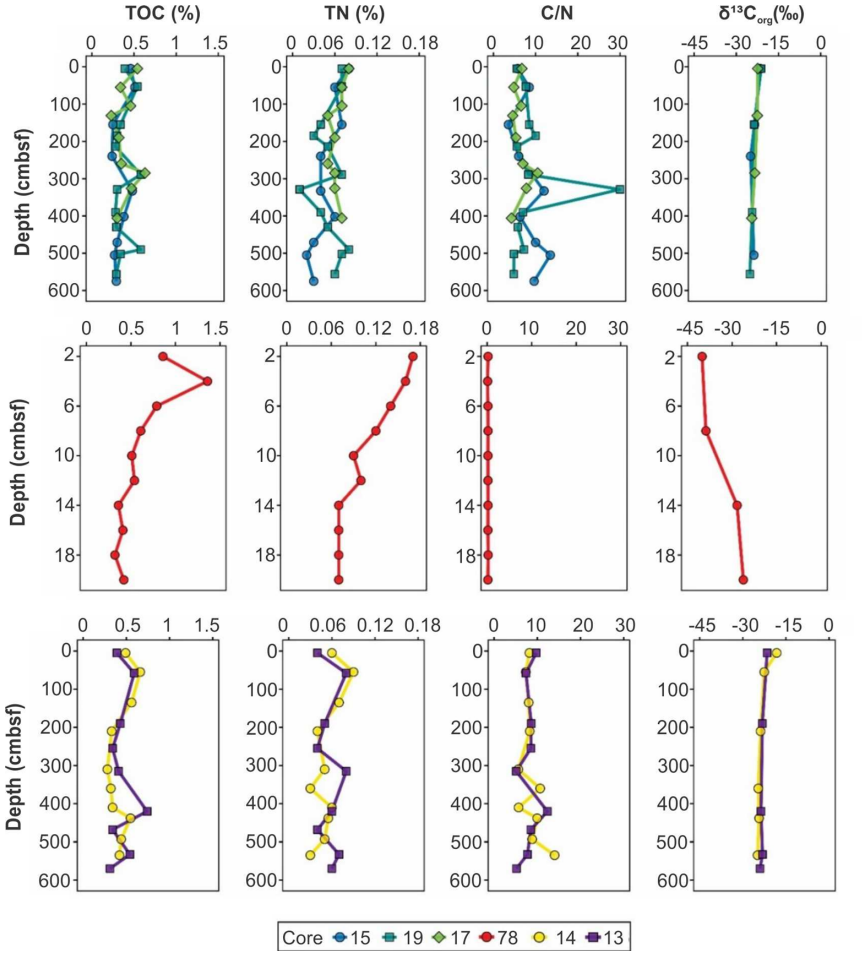

Figure 2. Downcore profiles of TOC, TN, C/N, and $\delta^{13}C_{org}$ in sediment cores. Profiles are arranged according to their position relative to the seep.

Linear regression analyses revealed covariation between TOC and TN, as well as potential coupling C/N ratios and $\delta^{13}C_{org}$ across sediment cores (Fig. 3). The strength of TOC–TN relationships varied among cores with the seep core exhibiting the highest correlation ($R^2 = 0.78$), cores 19 and 17 having the weakest correlations ($R^2 = 0.14–0.20$), and cores 15, 14, and 13 displaying intermediate values ($R^2 = 0.32–0.55$; Fig. 3a). When data from all cores were combined, TOC and TN showed a positive linear relationship ($R^2 = 0.60$; TN = 0.123 × TOC + 0.009; Fig. 3b). In contrast, C/N and $\delta^{13}C_{org}$ did not demonstrate meaningful covariation in cores 15, 19, 17, and 13 ($R^2 = 0–0.08$), whereas cores 14 and the seep core exhibited weak negative trends ($R^2 = 0.31–0.38$; Fig. 3c). Overall, data from all cores indicated no relationship between C/N and $\delta^{13}C_{org}$ ($R^2 = 0.002$; Fig. 3d).

https://doi.org/10.5194/egusphere-2026-5038
Preprint. Discussion started: 25 August 2026

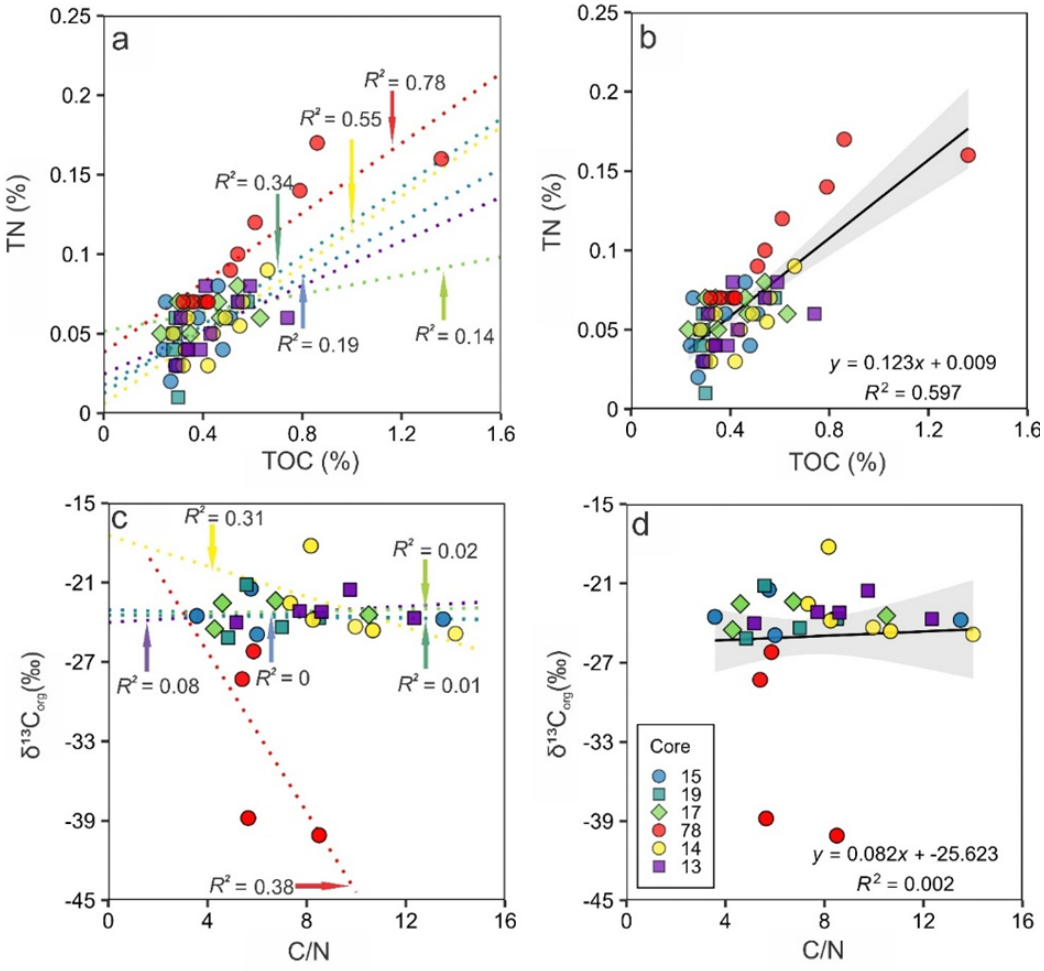

Figure 3. Spatial variation in TOC-TN and C/N-$\delta^{13}C_{org}$ coupling of sediment cores (a–d). For panels (a) and (c), colored arrows link R^2 values to their respective regression lines; confidence intervals are indicated by grey shaded regions on panels (b) and (d).

3.2. Porewater chemistry of sediment cores

Depth profiles of porewater ions (PO_4^{3-}, DIC, SO_4^{2-}, NH_4^+, NO_3^-, NO_2^-, Fe^{2+}, Mn^{2+}, and F^-) were combined with C/N ratios and core logs to evaluate porewater-sediment interactions (Fig. 4; Supplementary Tables S2, S3). In core 15, C/N peaked in deeper silty clays with rare bioturbation and organic-rich sand blebs. In cores 17 and 19, no relationship between downcore C/N profiles and lithologic variation is observed. However, cores 14 and 13 showed a pronounced increase in C/N ratios at 300–500 cmbsf, where organic-rich layers (ORLs) were detected (Fig. 4; Supplementary Fig.S7). Interestingly, in this interval, PO_4^{3-} concentration showed a pronounced peak in core 14, with concentrations ranging from 1 to 22 mmol·L^{-1}. Sulfate concentration decreased with sediment depths, while DIC continued to accumulate in deeper

https://doi.org/10.5194/egusphere-2026-5038
Preprint. Discussion started: 25 August 2026

sediments. The highest DIC concentration was recorded in The Hole, reaching ~12 mmol·L^{-1} compared to ~6.4 mmol·L^{-1} in non-seep cores, while surface SO_4^{2-} averaged 26.1 mmol·L^{-1} and was completely depleted at the core base. Only core 19 showed near-complete depletion of SO_4^{2-} with depth, while other cores had concentrations of 10 mmol·L^{-1} or less. NH_4^+ concentrations increased with depth, reaching about 1.5 mmol·L^{-1} in cores 14 and 13 and approximately 1 mmol·L^{-1} in other gravity cores. The Hole exhibited a lower maximum NH_4^+ concentration of ~0.7 mmol·L^{-1}. NO_3^- and NO_2^- concentrations were higher in the seep compared to the surrounding sediment cores and declined slightly with depth. Concentrations of Fe^{2+} and Mn^{2+} remained uniformly low (<0.2 mmol·L^{-1}) with no systematic downcore trends in most cores. Similarly, F^- showed no clear stratigraphic pattern and averaged 0.2 mmol·L^{-1}. Notably, Fe^{2+} and Mn^{2+} ions peaked in core 14 between the 200–500 cmbsl intervals, where NH_4^+ also continued to increase. Within this interval, ORLs have been reported, and a distinct SO_4^{2-}-DIC interaction was observed. In this regard, this interval (grey-shaded in Fig. 4) may represent a redox boundary where multiple terminal electron-accepting processes coexist.

https://doi.org/10.5194/egusphere-2026-5038
Preprint. Discussion started: 25 August 2026

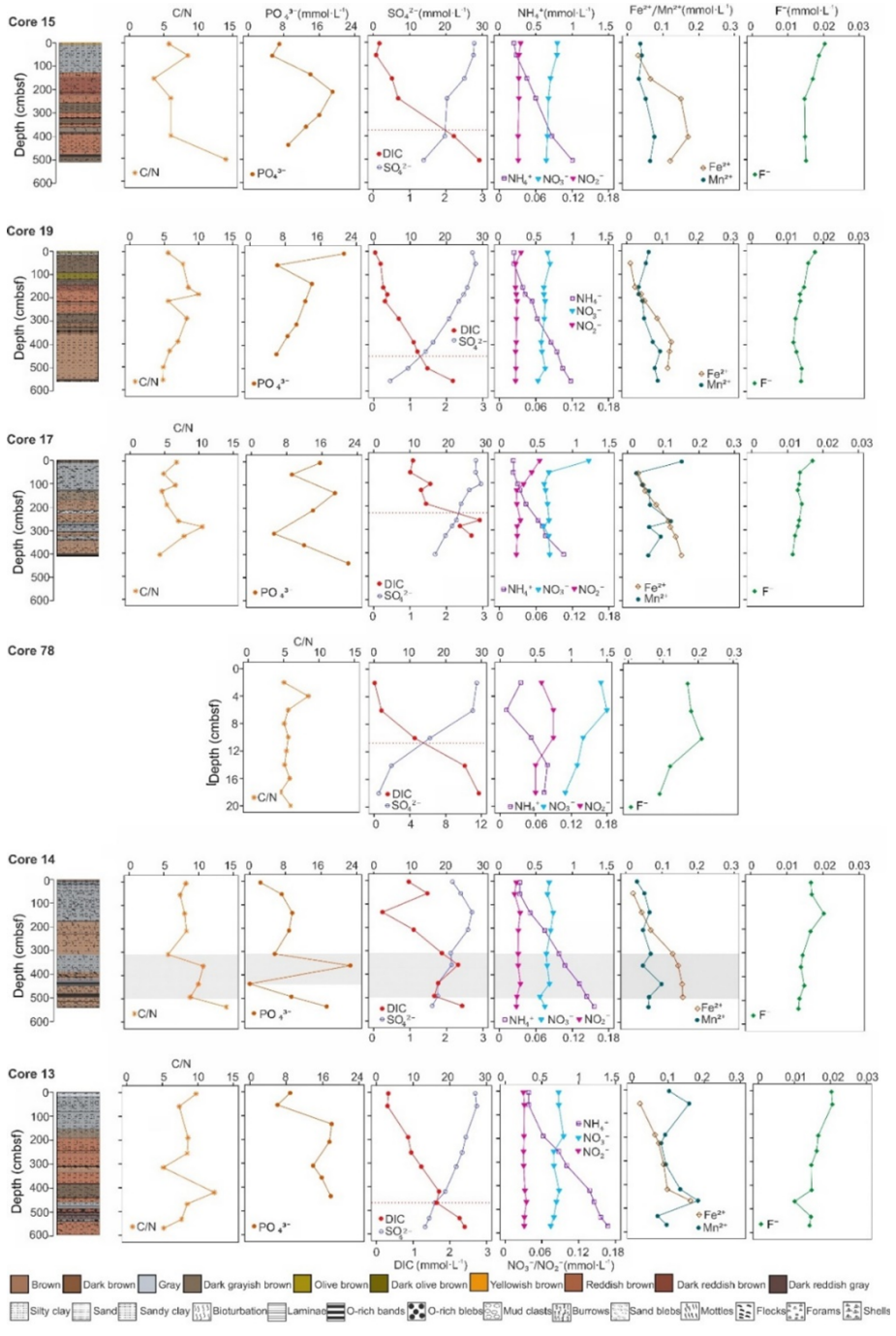

Figure 4. Lithological patterns (after Geological Survey Canada; GSC) and porewater geochemical profiles with sulfate-alkalinity transition zones marked by red dotted lines and biogeochemical zonation indicated by the gray-shaded interval in core 14.

https://doi.org/10.5194/egusphere-2026-5038
Preprint. Discussion started: 25 August 2026

3.3. Lipidomic survey

Identified archaeal CLs included glycerol dialkyl glycerol tetraethers (GDGTs) and archaeol (AR). The concentration of total isoprenoid GDGTs (*iso*GDGTs) ranged from 6.9 to 11.7 μg·g sed^{-1} in gravity cores, whereas substantially lower values were observed in The Hole (avg. 1.7 μg·g sed^{-1}). Hydroxy GDGTs (OH-GDGTs) occurred at lower concentrations, averaging 0.3 μg·g sed^{-1} in the seep and 0.8 μg·g sed^{-1} in other transect cores. Both *iso*GDGTs and OH-GDGTs were enriched in surface sediments and declined with depth (Fig. 5; Supplementary Table S4). The cyclopentane rings associated with *iso*GDGTs ranged from zero to five. Among these, *iso*GDGT-0, which lacks cyclopentane rings, and *iso*GDGT-5 (crenarchaeol), which contains one cyclohexane and four cyclopentane rings, were the dominant *iso*GDGTs in gravity cores and occurred in equal proportions. isoGDGT-1–3 were minor components in these cores but showed enrichment in the seep, particularly in the upper 10 cmbsf. Only OH-GDGTs with zero, one, or two cyclopentyl moieties (OH-GDGT-0–2) were detected along the transect (Fig. 6). AR concentrations were much lower than those of GDGTs, averaging 0.14 ± 0.04 μg·g sed^{-1} in all gravity cores and reaching a maximum concentration of 0.26 μg·g sed^{-1} in the seep. Hydroxylated AR (OH-AR) was absent in The Hole and, in other cores, averaged 0.09 ± 0.05 μg·g sed^{-1}, occurring at lower abundances than OH-GDGTs. Depth profiles of AR and OH-AR were spatially variable with no clear downcore pattern (Fig. 5).

Other detected archaeal membrane-spanning lipids included glycerol dibiphytanol diethers (GDDs), which have been considered either degradation products of *iso*GDGTs or biosynthetic compounds produced by archaea (Meador et al., 2014; Hingley et al., 2024; Supplementary Table S4). Similar to *iso*GDGTs, GDDs with 0–5 cyclopentyl rings were identified. Their hydroxylated counterparts (OH-GDDs) were also limited to 0–2 cyclopentyl moieties. GDD concentrations were consistently higher in surface sediments than in deeper layers, peaking at 1.25 μg·g sed^{-1} in surface core 14 and averaging 0.11 μg·g sed^{-1} within the seep. OH-GDDs occurred at lower concentrations, averaging 0.03 ± 0.01 μg·g sed^{-1} in gravity cores and 0.02 μg·g sed^{-1} at The Hole, without a clear downcore trend. GDD-0 and GDD-5 dominated all cores (15, 19, 17, 14, and 13), whereas GDD-1–3 contributed minor fractions, except for surface enrichment within The Hole (Figs. 5, 6).

Detected IPLs included mono- and di-glycosidic-GDGTs (1G-GDGTs and 2G-GDGTs, respectively) comprising 0–5 rings, with 1G-GDGTs being the most abundant IPLs, averaging 0.13 μg·g sed^{-1} in The Hole and 0.42 ± 0.09 μg·g sed^{-1} across gravity cores (Fig.5; Supplementary Table S4). In the seep, 1G-GDGTs containing 1–3 rings were particularly abundant. Detected hydroxylated 1G-GDGTs (1G-OH-GDGTs) and 2G-GDGTs (2G-OH-GDGTs) consisted only of 0–2 rings (Fig. 6). Additionally, we identified mono- and di-glycosidic ARs (1G- and 2G-AR), phosphatidic acid AR (PA-AR), and its hydroxylated analogue (PA-OH-AR). 1G-AR was detected in all cores and averaged 0.05 μg·g sed^{-1}, while 2G-AR was not detected in cores 15, 17, and 13. PA-AR occurred in only a few depth intervals at The Hole, averaging 0.01 μg·g sed^{-1}. In cores 15, 19, 17, and 14, PA-AR concentrations increased with depth, reaching 0.35 ± 0.06 μg·g sed-1. PA-OH-AR was restricted to cores 14 and 13, averaging 0.12 μg·g sed^{-1} and 0.03 μg·g sed^{-1}, respectively (Fig. 5; Supplementary Table S4).

Identified bacterial lipids included branched glycerol dialkyl glycerol tetraethers (*br*GDGTs; Supplementary Table S5). The average concentration of *br*GDGTs varied between 0.13 μg·g sed^{-1} and 0.9 μg·g sed^{-1}. In general, *br*GDGT-Ia and -IIa were the most abundant *br*GDGTs (accounting for 38% and 18 % of *br*GDGTs, respectively). Concentrations were highest in cores 15, 19, and 17, intermediate in cores 14 and 13, and lowest in core 13. *br*GDGT-Ic, -IIb, -IIc, -IIIb, and -IIIc were detected at the lowest concentrations in all cores, representing only 1–9% of *br*GDGTs (Figs. 5, 6).

Photosynthetic pigments, including chlorophyll *a* (Chl *a*), pheophytin *a* (Pheo *a*; a degradation product of Chl *a*), and their hydroxylated derivatives (OH-Chl *a* and OH-Pheo *a*), were monitored across all samples. Chl *a* peaked in core 14 (0.89 μg·g sed^{-1}) and reached the lowest concentration in core 19 (0.26 μg·g sed^{-1}). Pheo *a* recorded a lower concentration and averaged 0.07 ± 0.01 μg·g sed^{-1}. OH-Chl *a*

https://doi.org/10.5194/egusphere-2026-5038
Preprint. Discussion started: 25 August 2026

and OH-Pheo *a* averaged 0.03 ± 0.01 μg·g sed^{-1} each. In The Hole, Chl *a* and Pheo *a* were quantified at very low concentrations, while their hydroxylated derivatives were not detected. All pigments showed no clear stratigraphic patterns in their relative distributions (Fig. 5; Supplementary Table S5). Menaquinones with isoprenyl side chains containing four (MKs-4), six (MKs-6), seven (MKs-7), and ten (MKs-10) isoprene units and with different degrees of unsaturation of the side chain were also identified and quantified (Figs. 5, 6; Supplementary Table S6). MKs were below the detection limit in The Hole. The highest concentrations of MKs-4 were recorded in cores 15 and 14, averaging approximately 0.7 μg·g sed^{-1}. In contrast, MKs-10 were more abundant in cores 19, 17, and 13, with an average of 0.42 μg·g sed^{-1}. MKs-7 remained low across all cores, ranging from 0.05 to 0.17 μg·g sed^{-1}. MKs-6 showed strong enrichment in cores 14 and 13 (1.94 and 1.14 μg·g sed^{-1}, respectively), but were nearly absent in cores 15, 19, and 17. Among these, cores 14 and 13 were dominated by saturated MKs (MK-6:0 and MK-6:1; 68% of total MK-6).

https://doi.org/10.5194/egusphere-2026-5038
Preprint. Discussion started: 25 August 2026

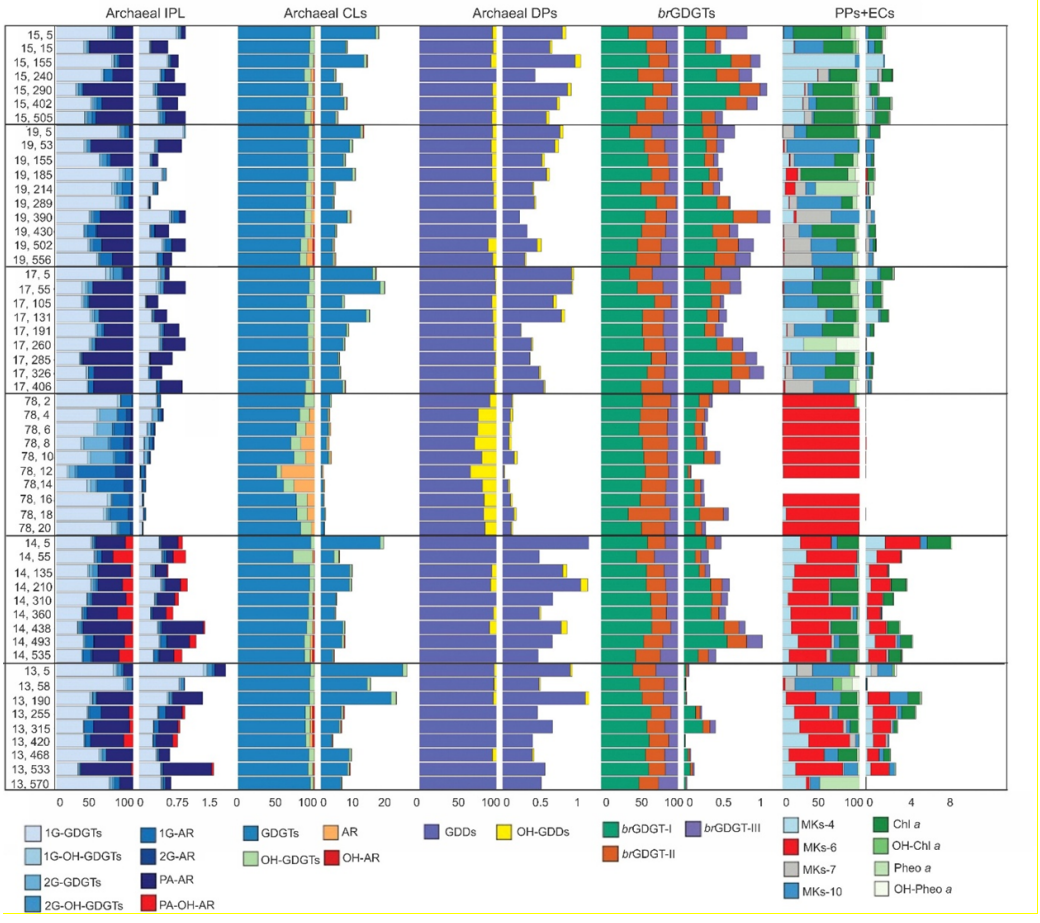

Figure 5. Depth-resolved profiles of archaeal lipids, bacterial *br*GDGTs, photosynthetic pigments (PPs), and electron carriers (ECs).

https://doi.org/10.5194/egusphere-2026-5038
Preprint. Discussion started: 25 August 2026

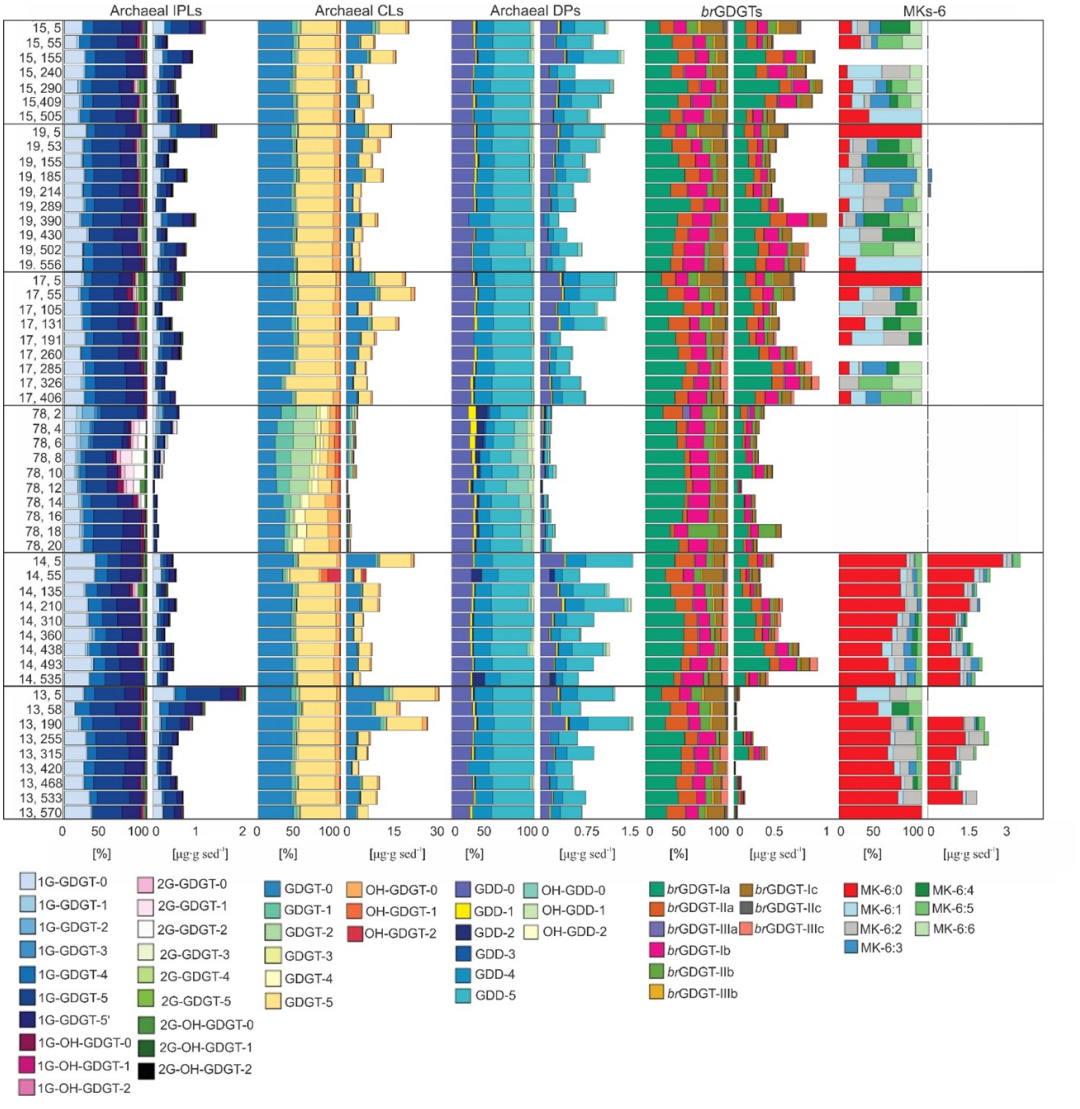

Figure 6. Downcore variation in archaeal lipid ring structures, *br*GDGTs, and MKs homologues.

4. Discussion

4.1. Organic matter sources and carbon inputs

4.1.1. Bulk geochemical constraints

Bulk geochemical analyses indicate differences in geochemical signature between The Hole and adjacent sediments (Figs. 2, 3; Supplementary Table S2). At The Hole, surface sediments are characterized by high TOC concentrations combined with strongly depleted $\delta^{13}C_{org}$ values, supporting active methane seepage that sustains microbial carbon processing (Joye et al., 2004; Joye, 2020; Redshaw et al., 2026). The ebullient CH_4 collected at The Hole exhibits a carbon isotopic composition of $\delta^{13}C$ = -71.0 ± 0.3‰

https://doi.org/10.5194/egusphere-2026-5038
Preprint. Discussion started: 25 August 2026

(Chowdhury et al., 2024), and the depleted $\delta^{13}C_{org}$ values closely match the isotopic signature of biogenic methane (Whiticar, 1999; Joye, 2020), indicating substantial methane-derived carbon input to the surface sediment organic matter pool. In contrast, $\delta^{13}C_{org}$ values across the transect (-25‰ to -21‰) fall within the typical range for marine organic matter (Meyers, 1994), suggesting minimal methane-derived carbon beyond The Hole. Fluctuations in C/N ratio in core 19 at 334 cmbsf, along with moderate fluctuations below approximately 300 cmbsf in cores 13 and 14, more likely reflect episodic terrestrial organic matter input or the selective diagenetic loss of nitrogen during burial, and the approximately 56% decline in TN at The Hole indicates progressive remineralization and early diagenetic transformation of organic matter (Wakeham, 2002; Redshaw et al., 2026). The variability in TOC-TN relationships (Fig. 3) highlights further site-specific controls on organic matter preservation and reveals pronounced spatial heterogeneity in organic matter sources and carbon cycling across the transect. These patterns occur alongside marked lithological variability among the cores, including differences in sand content, bioturbation, mottling, lamination, and organic-rich bands (Supplementary Fig. S7; Supplementary Table S2), which may influence organic matter deposition and preservation.

4.1.2. Photosynthetic contribution to sedimentary organic matter

The down-core preservation of photosynthetic pigments serves as an indicator of euphotic-zone contributions to the benthic organic matter pool. Localized pigment enrichments reflect periods of elevated primary productivity and the subsequent export of fresh phytoplankton material to the benthos (Jeffrey, 1974; Vernet & Lorenzen, 1987; Wernand et al., 2013). On the Scotian Slope, however, pigment variability is primarily modulated by post-depositional heterotrophic degradation and differences in organic matter preservation rather than initial export from the euphotic zone (Redshaw et al., 2026). Enrichment of MKs-4 in cores 14 and 15 coincides with the highest Chl *a* concentration across the transect. Specifically, MKs-4 averaged ~0.7 μg·g sed^{-1}, and Chl *a* reached 0.89 μg·g sed^{-1} in core 14, indicating enhanced input of phototroph-derived organic matter. While MKs are primarily associated with microbial producers, MK-4 is unique in that it occurs in cyanobacteria and phototrophic eukaryotes (Collins and Jones, 1981; Hiraishi, 1999). Its presence in Photosystem I of certain cyanobacteria (Gloeobacter violaceus, *Synechococcus sp*. PCC 7002), as well as in diatoms and primitive red algae (Nowicka and Kruk, 2010), further supports a phototrophic contribution to the MK-4 pool. The spatial association of MK-4 and Chl *a* (Supplementary Figs. S10, S11) therefore suggest enhanced deposition of relatively fresh phototroph-derived material at these cores, although contributions from heterotrophic MK-4 producers cannot be excluded.

Pigment concentrations vary with organic matter degradation as chlorophyll degradation products accumulate in sediments (Szymczak-Żyła and Kowalewska, 2011). The conversion of Chl *a* to Pheo *a* involves the removal of the central magnesium ion; while biologically catalyzed by enzymes during cellular senescence, this reaction occurs primarily via abiotic chemical pathways during early diagenesis, accelerated by thermal stress, acidification, bioturbation, and grazing pressure (Lajolo et al., 1971; Bianchi et al., 2000; Ingalls et al., 2000). Pheo *a* averaged 0.07 ± 0.01 μg·g sed^{-1}, while OH-Chl *a* and OH-Pheo *a* each averaged 0.03 ± 0.01 μg·g sed^{-1}. The consistently low concentrations of these degradation products and the absence of stratigraphic trends indicate a relatively uniform degradation regime. This degradation pathway is likely influenced by heterotrophic processes, with pigment loss generally enhanced under strong or fluctuating redox gradients (Sun et al., 1995; Ingalls et al., 2000). Low pigment concentrations at The Hole are consistent with enhanced heterotrophic degradation rather than reduced phytodetrital input. Pigment concentrations decrease downcore with TOC, indicating pigment loss during organic matter degradation (Redshaw et al., 2026). Outside the seep, higher pigment concentrations coincide with greater organic matter preservation, suggesting lower degradation rates in the surrounding sediments.

https://doi.org/10.5194/egusphere-2026-5038
Preprint. Discussion started: 25 August 2026

4.2. Microbial community structure and metabolic pathways

4.2.1. Ammonia oxidizing archaea

The enrichment of isoprenoidal electron carriers, specifically MK-6:0 and MK-6:1, in cores 14 and 13 (Fig. 6) aligns with localized AOA activity, as these specific MKs represent predominant components of Thaumarchaeota lipid matrices (Elling et al., 2016, 2017). Because MK-6 pools can exhibit taxonomic overlaps with distinct prokaryotic lineages, these structures cannot be unambiguously assigned to AOA on the basis of lipid profiles alone. However, their detection in deep-sediment archives down to 800 cmbsf, frequently exceeding water-column inventories, demonstrates the persistence of Thaumarchaeota biomarkers in deep-sediment environments. Their distribution is shaped by lithological and geochemical gradients, as well as increased heterotrophic activity (Becker et al., 2018). The presence of sediment-specific amoA lineages and genomic evidence of active subsurface populations further supports the in-situ production of Thaumarchaeota, rather than passive burial from the water column (Park et al., 2014; Ren et al., 2025). This niche establishment is likely energetically sustained by an inherently high oxygen affinity (Park et al., 2010) and, in distinct lineages, pathways for nitric oxide reduction (Bristow et al., 2016; Kraft et al., 2022). Consequently, the confinement of these MK signatures to cores 14 and 13, contrasted against their near absence in cores 15, 19, and 17, delineates a highly heterogeneous spatial mosaic of AOA activity regulated by localized redox boundaries, dissolved oxygen penetration, and NH_4^+ flux. Conversely, the absence of detectable MKs within the active seep site points to a divergent microbial regime (Figs. 5, 6, and Supplementary Fig. S11). This environment is potentially dominated by taxa utilizing alternative quinone profiles, or it is marked by accelerated quinone turnover under intensely reducing, high-flux conditions that preclude the accumulation of MK pools.

Elevated NH_4^+ concentrations in sediments significantly influence AOA diversity and activity, in addition to environmental factors such as temperature and salinity (He et al., 2018). Consistent with sediment-specific conditions, cores 14 and 13 exhibited the highest porewater NH_4^+ concentrations along the transect (Fig. 4; Supplementary Fig. S8). The strong correlation between MK-6:0 and NH_4^+ in core 14 (R^2 = 0.77) and the moderate correlation in core 13 (R^2 = 0.41) suggest that NH_4^+ availability is a primary determinant of thaumarchaeal quinone distribution in these sediments. In contrast, the weaker correlations observed in cores 15, 19, and 17 (R^2 = 0.06–0.25) suggest that additional environmental variables, including redox conditions and organic matter availability, also influence this relationship (Fig. 7). Collectively, these results highlight the spatial heterogeneity of Scotian Slope sediments, where varying geochemical conditions likely shape the composition of microbial assemblages.

https://doi.org/10.5194/egusphere-2026-5038
Preprint. Discussion started: 25 August 2026

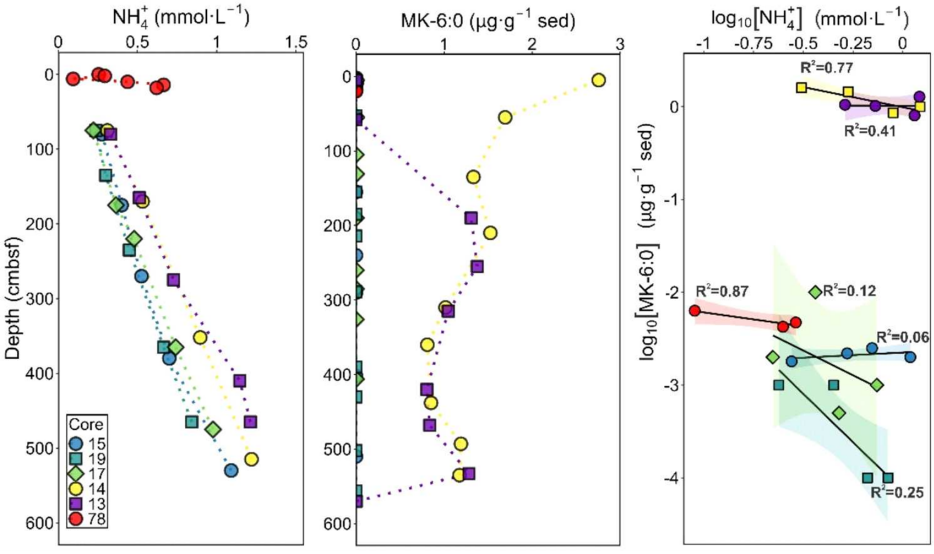

Figure 7. Downcore profiles of NH_4^+ and MK-6:0, along with their correlation patterns.

4.2.2. Methanotrophic Archaea

Lipid biomarkers indicate distinct spatial distributions of ANME clades. ANME-1 dominates the seep, as shown by the higher abundance of GDGT-1–3 (Fig. 6; Zhang et al., 2011, 2023), identifying this clade as the primary mediator of sulfate driven AOM (S-AOM) in The Hole (Redshaw et al., 2026). In contrast, cores 13 and 14 are characterized by enrichment of PA-OH-AR (Fig. 5; Supplementary Fig. S9), which may reflect either a distinct methanotrophic community or preferential preservation of these lipids. OH-AR/AR ratios remained ≤ 1 in cores 15, 19, and 17, consistent with an ANME-1-dominated community. Core 14 exhibited intermediate values of 1–2 between 150 and 400 cmbsf, whereas core 13 reached ratios approaching 2 below 500 cmbsf before generally declining to ≤ 1 at shallower depths (Fig. 8a). Low OH-AR/AR ratios (0–0.8) are characteristic of ANME-1, whereas higher values (1.1–5.5) indicate increasing contributions from ANME-2 and/or ANME-3 (Elvert et al., 2005; Niemann and Elvert, 2008). The distribution of OH-ARs in The Hole is also consistent with the ANME-1 archaeal lipid profile, which typically contains only trace amounts or no OH-ARs (Niemann and Elvert, 2008; Kurth et al., 2019). These patterns suggest spatial structuring of ANME communities across the transect. Significant correlations between AR and OH-AR were observed only in cores 13 ($R^2 = 0.82$, $p < 0.001$) and 14 ($R^2 = 0.72$, $p = 0.004$) (Fig. 8b), further supporting spatial differences in ANME lipid distributions.

Elevated NH_4^+ concentrations in cores 14 and 13 (Fig. 4; Supplementary Fig. S8) may reflect enhanced microbial remineralization and nitrogen cycling. One possible mechanism is AOM coupled to nitrate reduction, which can produce NH_4^+ through dissimilatory nitrate reduction to ammonium (DNRA), whereby NO_3^- is reduced to NO_2^- and subsequently to NH_4^+ (Haroon et al., 2013; Ettwig et al., 2016). Methane oxidation can also be coupled to the reduction of Fe and Mn oxides, providing alternative electron acceptors under appropriate redox conditions (Beal et al., 2009; Cai et al., 2018; Leu et al., 2020). In core 14, the discrete increases in Fe^{2+} and Mn^{2+} between 320 and 500 cmbsf (Fig.4; Supplementary Fig. S8) may indicate enhanced metal reduction and suggest that alternative electron-acceptor processes could contribute to methane cycling at these depths (Zhao et al., 2024; Xue et al.,

https://doi.org/10.5194/egusphere-2026-5038
Preprint. Discussion started: 25 August 2026

2025). However, the available geochemical data cannot resolve the specific microbial taxa or metabolic pathways responsible for these patterns; thus, a contribution from nitrate- or metal-coupled AOM remains hypothetical.

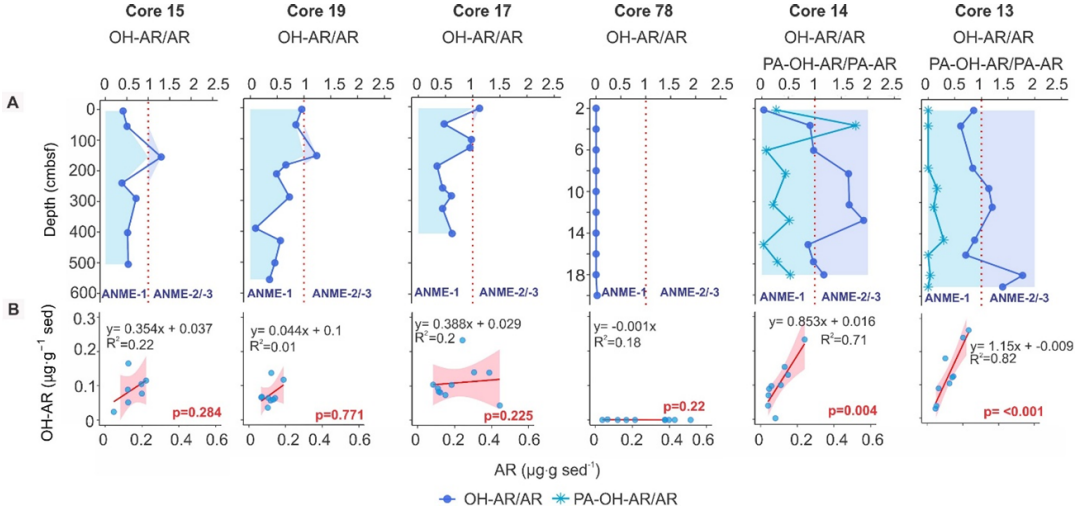

Figure 8: A) Depth profiles of the OH-AR/AR and PA-OH-AR/PA-AR ratios. B) Correlation between AR and OH-AR concentrations. The red dotted lines mark the boundary separating ANME-1 domain (light blue shaded area) and ANME-2 /-3 domain (dark blue shaded area).

4.2.3. Sulfate reducing bacteria

Sulfate-driven AOM at The Hole is indicated by the inverse relationship between SO_4^{2-} and DIC, which reflects active sulfate reduction and subsequent DIC accumulation (Antler et al., 2014; Hu et al., 2017; Redshaw et al., 2026). At this site, the sulfate-alkalinity transition zone (SATZ) was identified at a depth of 10 cmbsf (Redshaw et al., 2026). In contrast, adjacent cores did not exhibit complete SO_4^{2-} depletion (Fig. 4), suggesting either insufficient methane supply to drive full SO_4^{2-} reduction or the predominance of alternative electron acceptors. Cores 15, 19, and 17 exhibited increased concentrations of MKs-7 and *br*GDGTs in deeper sediment layers (Figs. 5, Supplementary Figs. S10, S11). Among the *br*GDGTs, *br*GDGT-Ia was most abundant, followed by *br*GDGT-IIa and *br*GDGT-IIIa (Fig. 6), which likely reflects preferential *in situ* microbial production rather than input from sedimentary sources. AOM appears to influence the relative abundances of *br*GDGT-Ia and *br*GDGT-IIa (Zhang et al., 2020; Zeng et al., 2025), thereby shaping specific microbial niches within the sediment column. Nevertheless, higher abundance of MKs-7 and *br*GDGTs in these cores provides only indirect evidence for sulfate reduction. MKs-7 are not unique to sulfate-reducing bacteria, as quinone composition varies substantially even within sulfate-reducing lineages (Suzuki et al., 2008; Song et al., 2021). Similarly, *br*GDGTs were enriched in the seep sediments, with the highest concentrations observed at the base of The Hole. This enrichment is consistent with previous observations linking *br*GDGT-Ia, -IIa, and -IIb to enhanced AOM and sulfate-reducing bacterial communities in cold seep environments (Zhang et al., 2024; Redshaw et al., 2026). Thus, the *br*GDGT signal may reflect microbial activity associated with methane cycling at the seep.

https://doi.org/10.5194/egusphere-2026-5038
Preprint. Discussion started: 25 August 2026

4.3. The relationship amongst microbial communities

Multivariate analyses, including HCA and PCA, were conducted to investigate relationships among microbial communities in the seep and adjacent gravity cores. HCA identified seven lipidomes (L) and six lipid classes (LC), revealing differences in microbial community structure (Fig. 9). LC-1a and -1b were enriched in archaeal IPLs and CLs. LC-1a was primarily associated with surface sediments of cores 15, 19, 17, 14, and 13, while LC-1b was strongly associated with The Hole and dominated by *iso*GDGTs and glycosidic GDGTs characteristic of ANME-1 archaea, consistent with active AOM. LC-2 consisted mainly of photosynthetic pigments enriched at the SWI of all cores, reflecting inputs from surface primary production. LC- 3 was also enriched in archaeal IPLs and CLs, primarily in the surface sediments of cores 15, 19, 17, 14, and 13. LC- 4, characterized by *br*GDGTs and MK-7 homologues, exhibited a heterogeneous distribution across the gravity cores but was least abundant in the seep. LC- 5 comprised hydroxylated GDGTs without a clear spatial pattern. LC- 6 was dominated by MK-6 homologues, particularly in cores 13 and 14 and mainly within lipidomes 3 and 7, suggesting enhanced respiratory activity associated with AOA. PCA was performed separately for porewater data combined with lipid classes categorized as (a) photosynthetic pigments, (b) MKs, (c) *br*GDGTs, and (d) archaeal IPLs and CLs (Fig. 10). The Hole formed a distinct cluster, indicating a unique combination of porewater geochemistry and microbial lipid composition, whereas cores 15, 19, 17, 14, and 13 exhibited variable associations depending on the lipid class. Both HCA and PCA revealed distinct microbial lipid signatures between the seep and adjacent sediments, consistent with contrasting geochemical conditions and microbial assemblages.

https://doi.org/10.5194/egusphere-2026-5038
Preprint. Discussion started: 25 August 2026

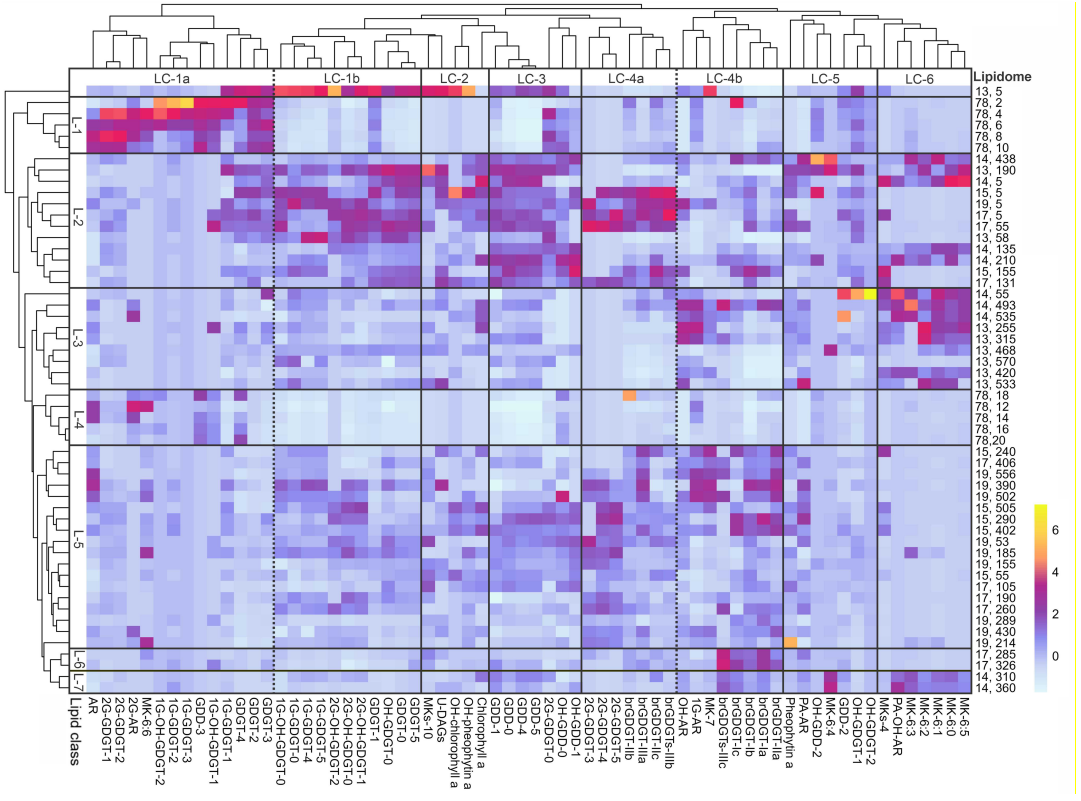

Figure 9: Hierarchical cluster analysis heatmap with dendrogram showing the z-scored concentrations of all detected lipids across the transect. Rows represent core samples, L represents lipidomes and LC represents lipid classes.

https://doi.org/10.5194/egusphere-2026-5038
Preprint. Discussion started: 25 August 2026

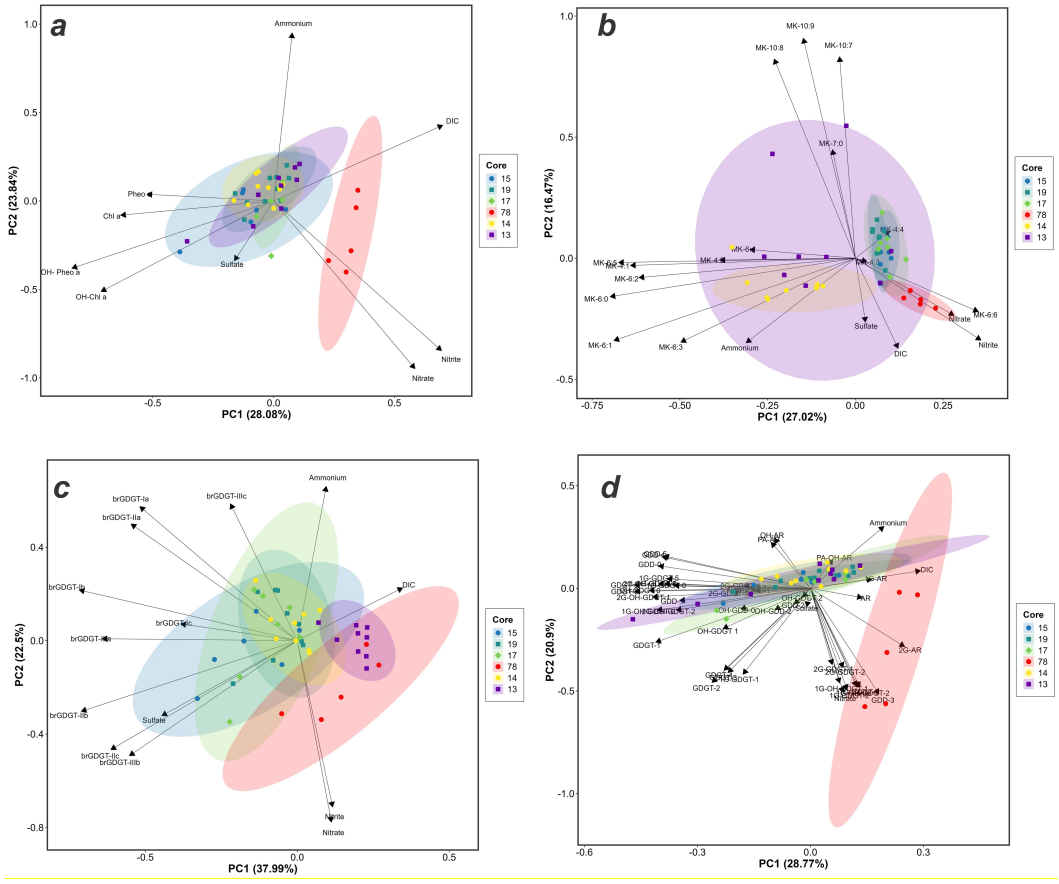

Figure 10: Principal component analysis of porewater ions and lipid classes, including a) photosynthetic pigments, b) MKs, c) *br*GDGTs, and d) archaeal IPLs and CLs.

4.4. Sedimentary and geological controls on biogeochemical dynamics and microbial assemblages

Recent lipidomic analyses at Site 2A-1 have revealed fine-scale microbial zonation within seep sediments (Redshaw et al., 2026). The distinct lipidomic and geochemical signatures observed across the transect further highlight the role of spatial differences in geological setting and fluid-plumbing systems in shaping microbial distributions across the study area (Fig. 11; Supplementary Fig. S3). The Hole is an actively venting methane cold seep sustained by focused fluid flux above the diapir crest (Chowdhury et al. 2024). Crustal faults in this region serve as high-permeability conduits for methane transport from the deep biosphere (Fig. 1; Supplementary Figs. S2, S3), supporting elevated heterotrophic activity, intense sulfate reduction, and active AOM, consistent with a primary fault-controlled seep pathway (Chowdhury et al., 2024; Redshaw et al., 2026). In contrast, cores 15, 19, and 17 reflect background marine sedimentation. These sites exhibit intermediate sulfate reduction, low-to-moderate heterotrophic activity, and limited microseepage, indicating diffuse, low-intensity methane input rather than focused subsurface

https://doi.org/10.5194/egusphere-2026-5038
Preprint. Discussion started: 25 August 2026

fluid advection. Cores 14 and 13 occupy an intermediate structural position along the diapir margin, where secondary faults associated with salt dissolution and growth faulting may facilitate localized migration of hydrocarbon- and nutrient-rich brines. Elevated NH_4^+ concentrations and high C/N ratios at these sites support potentially a brine-derived nitrogen contribution (Stüeken et al., 2024). Increased NH_4^+ availability likely influences the community structure of AOA and their associated lipid biomarkers (Francis et al., 2005; Sintes et al., 2016). Within this probable brine-influenced flow regime, S-AOM likely occurs in discrete horizons rather than throughout the sediment column. Under these conditions, S-AOM likely remains active but is spatially constrained. This constraint allows AOM coupled to iron and manganese reduction (Beal et al., 2009) or nitrogen cycling (Ettwig et al., 2010). Core 13 represents a transitional setting with a weaker manifestation of these processes despite its proximity to the diapir (Fig. 11).

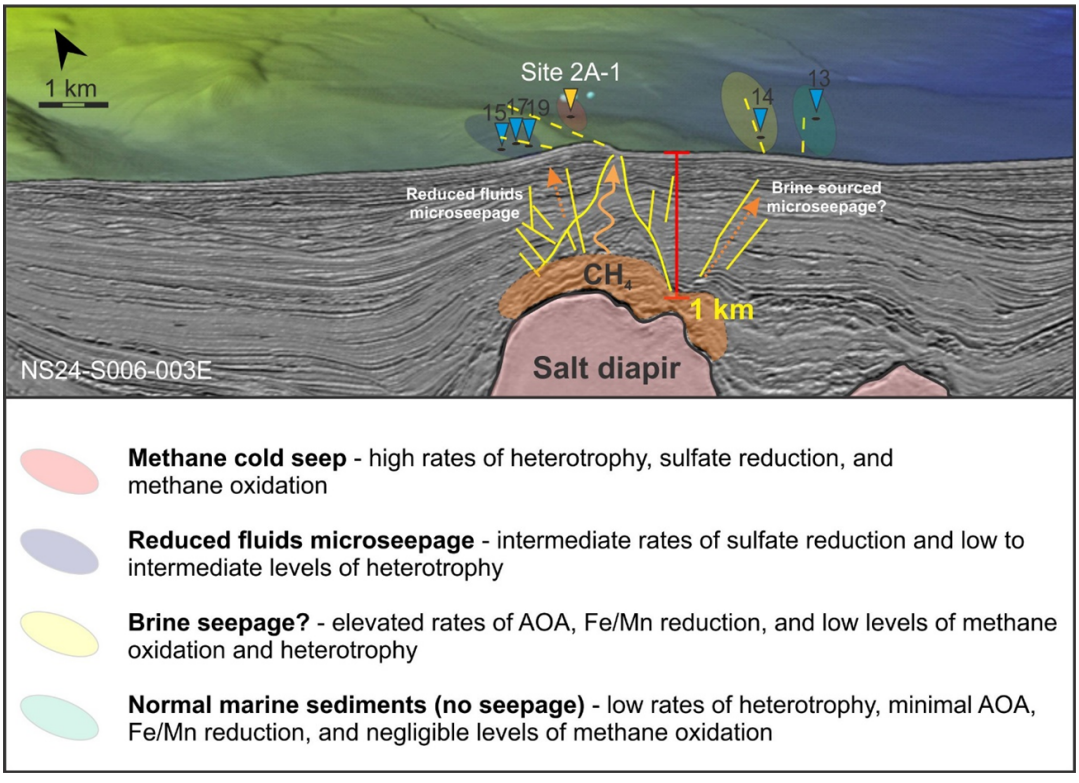

Figure 11: Three-dimensional seismic bathymetric map and seismic crossline of the survey region (modified from Redshaw et al., 2026) showing surface sediment microbial shifts in response to subsurface geological structures and seepage. Yellow lines mark radial and crustal faults overlying the salt diapir (orientation of seismic section produces different fault spays from Fig. 1). The orange region traces the generalized region for the seep's primary methane source (with an orange arrow illustrating the gas migration pathway; Chowdhury et al., 2024). Images provided courtesy of the NSDoE.

https://doi.org/10.5194/egusphere-2026-5038
Preprint. Discussion started: 25 August 2026

5. Conclusion

This study provides a comprehensive biogeochemical, lipidomic, and sedimentological survey that demonstrates deeply buried geologic structures producing cold seeps can also alter the surrounding, regional shallow sedimentary environment well beyond obvious ocean-floor seep structures. Three ecologically and metabolically distinct microbial assemblages were identified, dominated by AOA, ANMEs, and SRB, each corresponding to discrete redox niches shaped by geological factors. At the methane seep, a distinct geochemical signature indicative of active AOM was detected, with ANME-1 as the predominant microbial population. In contrast, sediments associated with reduced microseepage sources exhibited no unique geochemical patterns and primarily reflected background sedimentary conditions. Cores collected above the buried salt diapir revealed a tightly coupled redox network that linked multiple electron acceptors to a compositionally unique microbial assemblage. The spatial alignment between this assemblage and the underlying salt structure suggests diffusive microseepage along deep fault conduits is the primary mechanism sustaining microbial activity in this region. Seismic reflection data show these variations, which, in several cases, occur in seemingly monotonous, normal marine slope sediments, are directly above rock strata linked to a larger, complex radial fault system formed by the intrusion of a deeply buried salt diapir. These results enhance our understanding of how subsurface salt diapirism influences geochemical gradients that organize benthic microbial communities and highlight the importance of a multi-proxy framework for linking subsurface geological processes to near-surface biogeochemical cycling.

Author contribution

GO and GTV designed the research and wrote the manuscript. GO generated the lipid data and provided the data analysis. UU provided technical support with lipid identification. NM provided geographical data. PG provided tech support for lipid analyses. AM provided logistical support for sampling and project completion. ER and PG provided analytical support with bulk geochemistry and molecular analyses. CC led the 2018 expedition and provided support for sedimentological descriptions. JVB provided technical support for porewater analysis.

Competing interests

The authors declare that they have no conflict of interest.

Acknowledgments

Thanks to the Nova Scotia Provincial Government for support of this project and, along with Natural Resources Canada, spear-heading the various research cruises and surveys that made the integrative data collection possible. A special thanks is given to Carey Ryan of Net Zero Atlantic, who was the GAPP Partnership Program manager responsible for the larger group research initiatives. Carey also managed the procuration and organization of the research cruises. We would also like to acknowledge that Julius Lipp, Florence Schubotz, and Kai-Uwe Hinrichs of MARUM, University of Bremen were instrumental in helping to first develop SMU's techniques in lipidomics. An additional special thanks is given to Kim Doane, the executive director of the Subsurface and Offshore Energy Branch of the Department of Energy for her support of the Organic Geochemistry Research Group at Saint Mary's University. Sediment samples analysed in this study were collected during three marine field programs led by Natural Resources Canada- Geological Survey of Canada under a joint collaborative research agreement with Nova Scotian Department of Natural Resources and Renewables. Kate Jarrett of Natural Resources Canada provided the core logs that were used to describe the sediment lithologies used for the study. Nikita Lakhanpal provided porewater analyses for this study.

https://doi.org/10.5194/egusphere-2026-5038
Preprint. Discussion started: 25 August 2026

Financial support

Funding for this project was sourced from: Genome Atlantic and Genome Canada; Research Nova Scotia (grant no. 2142); Mitacs (grant no. IT12481 and IT29547), NetZero Atlantic, the Natural Sciences and Engineering Research Council of Canada (grant no. RGPIN-2018-06147; NSERC), NSERC Canada Research Chairs (CRC) program, Canada Foundation for Innovation (CFI; JELF–CRC, John R. Evans Leaders Fund), and NSERC Discovery Grants program (application no. RGPIN-2017-05822).

References

Ahangarian, N., Umoh, U. U., MacAdam, N., MacDonald, A., Granados, P., Bentley, J. N., Redshaw, E., Fowler, M. G., Baghalabadi, V., and Ventura, G. T.: Archaeal lipostratigraphy of the Scotian Slope shallow sediments, Atlantic Canada, Biogeosciences, 23, 21–38, https://doi.org/10.5194/bg-23-21-2026, 2026.

Albertz, M., Beaumont, C., Shimeld, J. W., Ings, S. J., and Gradmann, S.: An investigation of salt tectonic structural styles in the Scotian Basin, offshore Atlantic Canada: 1. Comparison of observations with geometrically simple numerical models, Tectonics, 29, TC4017, https://doi.org/10.1029/2009TC002539, 2010.

Antler, G., Turchyn, A. V., Herut, B., Davies, A., Rennie, V. C. F., and Sivan, O.: Sulfur and oxygen isotope tracing of sulfate driven anaerobic methane oxidation in estuarine sediments, Estuar. Coast. Shelf Sci., 142, 4–11, https://doi.org/10.1016/j.ecss.2014.03.001, 2014.

Beal, E. J., House, C. H., and Orphan, V. J.: Manganese- and iron-dependent marine methane oxidation, Science, 325, 184–187, https://doi.org/10.1126/science.1169984, 2009.

Becker, K. W., Elling, F. J., Schröder, J. M., Lipp, J. S., Goldhammer, T., Zabel, M., Elvert, M., Overmann, J., and Hinrichs, K.-U.: Isoprenoid quinones resolve the stratification of redox processes in a biogeochemical continuum from the photic zone to deep anoxic sediments of the Black Sea, Appl. Environ. Microbiol., 84, e02736-17, https://doi.org/10.1128/AEM.02736-17, 2018.

Bentley, J. N., Ventura, G. T., Walters, C. C., Sievert, S. M., and Seewald, J. S.: The influence of near-surface sediment hydrothermalism on the TEX86 tetraether-lipid-based proxy and a new correction for ocean bottom lipid overprinting, Biogeosciences, 19, 4459–4477, https://doi.org/10.5194/bg-19-4459-2022, 2022.

Bennett, R. and Desiage, P.-A.: Expedition report 21CONDOR: Scotian Slope, 14–29 August 2021 (Open File 8889, Geological Survey of Canada, 2022), https://doi.org/10.4095/329977, 2022.

Bianchi, T. S., Johansson, B., and Elmgren, R.: Breakdown of phytoplankton pigments in Baltic sediments: effects of anoxia and loss of deposit-feeding macrofauna, J. Exp. Mar. Biol. Ecol., 251, 161–183, https://doi.org/10.1016/S0022-0981(00)00212-4, 2000.

Bligh, E. G. and Dyer, W. J.: A Rapid Method of Total Lipid Extraction and Purification, Can. J. Biochem. Physiol., 37, 911–917, 1959.

Boetius, A., Ravenschlag, K., Schubert, C. J., Rickert, D., Wid del, F., Gieseke, A., Amann, R., Jørgensen, B. B., Witte, U., and Pfannkuche, O.: A marine microbial consortium apparently mediating anaerobic oxidation of methane, Nature, 407, 623–626, https://doi.org/10.1038/35036572, 2000.

Bristow, L. A., Dalsgaard, T., Tiano, L., Mills, D. B., Bertagnolli, A. D., Wright, J. J., Hallam, S. J., Ulloa, O., Canfield, D. E., Revsbech, N. P., and Thamdrup, B.: Ammonium and nitrite oxidation at nanomolar oxygen concentrations in oxygen minimum zone waters, Proc. Natl. Acad. Sci. USA, 113, 10601–10606, https://doi.org/10.1073/pnas.1600359113, 2016.

Cai, C., Leu, A. O., Xie, G.-J., Guo, J., Feng, Y., Zhao, J.-X., Tyson, G. W., Yuan, Z., and Hu, S.: A methanotrophic archaeon couples anaerobic oxidation of methane to Fe(III) reduction, ISME J., 12, 1929–1939, https://doi.org/10.1038/s41396-018-0109-x, 2018.

https://doi.org/10.5194/egusphere-2026-5038
Preprint. Discussion started: 25 August 2026

Campbell, D. C.: CCGS Hudson Expedition 2016-011, phase 2. Cold seep investigations on the Scotian Slope, offshore Nova Scotia, 15 June–6 July 2016 (Geological Survey of Canada, Open File, 8525), https://doi.org/10.4095/313603, 2019.

Campbell, D. C. and Normandeau, A.: CCGS Hudson Expedition 2018-041: high-resolution investigation of deep-water seabed seeps and landslides along the Scotian Slope, offshore Nova Scotia, May 26–June 15, 2018 (Geological Survey of Canada, Open File, 8567), https://doi.org/10.4095/314695, 2019.

Campbell, C., Normandeau, A., Fraser, P., and MacDonald, A.: Detailed geomorphology of cold seeps associated with a buried salt diapir, offshore Nova Scotia, Canada (EGU General Assembly 2020, EGU2020-9901), 2020.

Craig, H.: Isotopic standards for carbon and oxygen and correction factors for mass-spectrometric analysis of carbon dioxide, Geochim. Cosmochim. Acta, 12, 133–149, 1957.

Chevalier, N., Bouloubassi, I., Stadnitskaia, A., Taphanel, M.-H., and Sinninghe Damsté, J. S.: Lipid biomarkers for anaerobic oxidation of methane and sulphate reduction in cold seep sediments of Nyegga pockmarks (Norwegian margin): discrepancies in contents and carbon isotope signatures, Geo-Mar. Lett., 34, 269–280, https://doi.org/10.1007/s00367-014-0363-5, 2014.

Chowdhury, A., Ventura, G. T., Owino, Y., Lalk, E. J., MacAdam, N., Dooma, J. M., Ono, S., Fowler, M., MacDonald, A., Bennett, R., MacRae, R. A., Hubert, C. R. J., Bentley, J. N., and Kerr, M. J.: Cold seep formation from salt diapir–controlled deep biosphere oases, Proc. Natl. Acad. Sci. U.S.A., 121, e2316878121, https://doi.org/10.1073/pnas.2316878121, 2024.

Collins, M. D., and Jones, D.: Distribution of isoprenoid quinone structural types in bacteria and their taxonomic implication, Microbiol. Rev., 45, 316–354, https://doi.org/10.1128/mr.45.2.316-354.1981, 1981.

Deptuck, M. E., and Kendell, K. L.: Chapter 13 – A review of Mesozoic-Cenozoic salt tectonics along the Scotian Margin, eastern Canada, in Permo-Triassic Salt Provinces of Europe, North Africa and the Atlantic Margins, Soto, J. I., Flinch, J. F., and Tari, G. (Eds.), Elsevier, 287–312, https://doi.org/10.1016/B978-0-12-809417-4.00014-8, 2017.

Dong, X., Rattray, J. E., Campbell, D. C., Webb, J., Chakraborty, A., Adebayo, O., Matthews, S., Li, C., Fowler, M., Morrison, N. M., MacDonald, A., Groves, R. A., Lewis, I. A., Wang, S. H., Mayumi, D., Greening, C., and Hubert, C. R. J.: Thermogenic hydrocarbon biodegradation by diverse depth-stratified microbial populations at a Scotian Basin cold seep, Nat. Commun., 11, 5825, https://doi.org/10.1038/s41467-020-19648-2, 2020.

Elling, F. J., Becker, K. W., Könneke, M., Schröder, J. M., Kellermann, M. Y., Thomm, M., and Hinrichs, K.-U.: Respiratory quinones in Archaea: phylogenetic distribution and application as biomarkers in the marine environment, Environ. Microbiol., 18, 692–707, https://doi.org/10.1111/1462-2920.13086, 2016.

Elling, F. J., Könneke, M., Nicol, G. W., Stieglmeier, M., Bayer, B., Spieck, E., De La Torre, J. R., Becker, K. W., Thomm, M., Prosser, J. I., Herndl, G. J., Schleper, C., and Hinrichs, K.: Chemotaxonomic characterisation of the thaumarchaeal lipidome, Environ. Microbiol., 19, 2681–2700, https://doi.org/10.1111/1462-2920.13759, 2017.

Ettwig, K. F., Butler, M. K., Le Paslier, D., Pelletier, E., Mangenot, S., Kuypers, M. M. M., Schreiber, F., Dutilh, B. E., Zedelius, J., de Beer, D., Gloerich, J., Wessels, H. J. C. T., van Alen, T., Luesken, F., Wu, M. L., van de Pas-Schoonen, K. T., Op den Camp, H. J. M., Janssen-Megens, E. M., Francoijs, K.-J., Stunnenberg, H., Weissenbach, J., Jetten, M. S. M., and Strous, M.: Nitrite-driven anaerobic methane oxidation by oxygenic bacteria, Nature, 464, 543–548, https://doi.org/10.1038/nature08883, 2010.

Ettwig, K. F., Zhu, B., Speth, D., Keltjens, J. T., Jetten, M. S. M., and Kartal, B.: Archaea catalyze iron-dependent anaerobic oxidation of methane, Proc. Natl. Acad. Sci. USA, 113, 12792–12796, https://doi.org/10.1073/pnas.1609534113, 2016.

Elvert, M., Hopmans, E. C., Treude, T., Boetius, A., and Suess, E.: Spatial variations of methanotrophic consortia at cold methane seeps: implications from a high-resolution molecular and isotopic approach, Geobiology, 3, 195–209, https://doi.org/10.1111/j.1472-4669.2005.00051.x, 2005.

Foucher, J. P., Westbrook, G. K., Boetius, A., Ceramicola, S., Dupré, S., Mascle, J., Mienert, J., Pfannkuche, O., Pierre, C., and Praeg, D.: Structure and drivers of cold seep ecosystems, Oceanography, 22, 92–109, https://doi.org/10.5670/oceanog.2009.11, 2009.

https://doi.org/10.5194/egusphere-2026-5038
Preprint. Discussion started: 25 August 2026

Fowler, M., Webb, J., Gulbrandsen, S., Austnes, L.-K., and Ashraf, F.: Geochemistry Data Report for 2018 Scotian Slope Coring Program, available online at: https://oera.ca/sites/default/files/2019-05/Geochemistry%20Data%20Report%20for%202018%20Scotian%20Slope%20Coring%20Program.pdf, 2018.

Francis, C. A., Roberts, K. J., Beman, J. M., Santoro, A. E., and Oakley, B. B.: Ubiquity and diversity of ammonia-oxidizing archaea in water columns and sediments of the ocean, Proc. Natl. Acad. Sci. USA, 102, 14683–14688, https://doi.org/10.1073/pnas.0506625102, 2005.

Gittins, D. A., Desiage, P.-A., Morrison, N., Rattray, J. E., Bhatna gar, S., Chakraborty, A., Zorz, J., Li, C., Horanszky, O., Cramm, M.A., Bisiach, F., Bennett, R., Webb, J., MacDonald, A., Fowler, M., Campbell, D. C., and Hubert, C. R. J.: Geological pro cesses mediate a microbial dispersal loop in the deep biosphere, Sci. Adv., 8, eabn3485, https://doi.org/10.1126/sciadv.abn3485, 2022.

Haroon, M. F., Hu, S., Shi, Y., Imelfort, M., Keller, J., Hugenholtz, P., Yuan, Z., and Tyson, G. W.: Anaerobic oxidation of methane coupled to nitrate reduction in a novel archaeal lineage, Nature, 500, 567–570, https://doi.org/10.1038/nature12375, 2013.

Hinrichs, K.-U., Hayes, J. M., Sylva, S. P., Brewer, P. G., and DeLong, E. F.: Methane-consuming archaebacteria in marine sediments, Nature, 398, 802–805, https://doi.org/10.1038/19751, 1999.

Hiraishi, A.: Isoprenoid quinones as biomarkers of microbial populations in the environment, J. Biosci. Bioeng., 88, 449–460, https://doi.org/10.1016/S1389-1723(00)87658-6, 1999.

Hu, C.-Y., Frank Yang, T., Burr, G. S., Chuang, P.-C., Chen, H.-W., Walia, M., Chen, N.-C., Huang, Y.-C., Lin, S., Wang, Y., Chung, S.-H., Huang, C.-D., and Chen, C.-H.: Biogeochemical cycles at the sulfate-methane transition zone (SMTZ) and geochemical characteristics of the pore fluids offshore southwestern Taiwan, J. Asian Earth Sci., 149, 172–183, https://doi.org/10.1016/j.jseaes.2017.07.002, 2017.

Ingalls, A. E., Aller, R. C., Lee, C., and Sun, M.-Y.: The influence of deposit-feeding on chlorophyll-a degradation in coastal marine sediments, J. Mar. Res., 58, 631–651, 2000.

Jeffrey, S. W.: Profiles of photosynthetic pigments in the ocean using thin-layer chromatography, Mar. Biol., 26, 101–110, https://doi.org/10.1007/BF00388879, 1974.

Jørgensen, B. B., and Boetius, A.: Feast and famine – microbial life in the deep-sea bed, Nat. Rev. Microbiol., 5, 770–781, https://doi.org/10.1038/nrmicro1745, 2007.

Joye, S. B., Boetius, A., Orcutt, B. N., Montoya, J. P., Schulz, H. N., Erickson, M. J., et al.: The anaerobic oxidation of methane and sulfate reduction in sediments from Gulf of Mexico cold seeps, Chem. Geol., 205, 219–238, https://doi.org/10.1016/j.chemgeo.2003.12.019, 2004.

Joye, S. B.: The geology and biogeochemistry of hydrocarbon seeps, Annu. Rev. Earth Planet. Sci., 48, 205–231, https://doi.org/10.1146/annurev-earth-063016-020052, 2020.

Judd, A., and Hovland, M.: Seabed fluid flow: the impact on geology, biology and the marine environment, Cambridge University Press, Cambridge, https://doi.org/10.1017/CBO9780511535918, 2007.

Kahn, L.: Determination of total organic carbon in sediment, U.S. Environmental Protection Agency, Region II, Environmental Services Division, Edison, New Jersey, 1988.

Knittel, K. and Boetius, A.: Anaerobic oxidation of methane: progress with an unknown process, Annu. Rev. Microbiol., 63, 311–334, https://doi.org/10.1146/annurev.micro.61.080706.093130, 2009.

Knittel, K., Lösekann, T., Boetius, A., Kort, R., and Amann, R.: Diversity and distribution of methanotrophic archaea at cold seeps, Appl. Environ. Microbiol., 71, 467–479, https://doi.org/10.1128/AEM.71.1.467-479, 2005.

Kraft, B., and Canfield, D. E.: Microbe profile: Nitrosopumilus maritimus, Microbiology, 168, 001207, https://doi.org/10.1099/mic.0.001207, 2022.

Kurth, J. M., Smit, N. T., Berger, S., Schouten, S., Jetten, M. S. M., and Welte, C. U.: Anaerobic methanotrophic archaea of the ANME-2d clade feature lipid composition that differs from other ANME archaea, FEMS Microbiol. Ecol., 95, fiz082, https://doi.org/10.1093/femsec/fiz082, 2019.

https://doi.org/10.5194/egusphere-2026-5038
Preprint. Discussion started: 25 August 2026

LaJolo, F. M., Tannenbaum, S. R., and Labuza, T. P.: Reaction at limited water concentration. 2. Chlorophyll degradation, J. Food Sci., 36, 850–853, https://doi.org/10.1111/j.1365-2621.1971.tb15542.x, 1971.

Leu, A. O., McIlroy, S. J., Ye, J., Parks, D. H., Orphan, V. J., and Tyson, G. W.: Lateral gene transfer drives metabolic flexibility in the anaerobic methane-oxidizing archaeal family Methanoperedenaceae, mBio, 11, e01325-20, https://doi.org/10.1128/mBio.01325-20, 2020.

Levin, L. A.: Ecology of cold seep sediments: interactions of fauna with flow, chemistry and microbes, Oceanogr. Mar. Biol. Annu. Rev., 43, 1–46, 2005.

Li, C., Adebayo, O., Ferguson, D. K., Wang, S., Rattray, J. E., Fowler, M., Webb, J., Campbell, C., Morrison, N., MacDonald, A., and Hubert, C. R. J.: Bacterial anomalies associated with deep sea hydrocarbon seepage along the Scotian Slope, Deep-Sea Res. I: Oceanogr. Res. Pap., 193, 103955, https://doi.org/10.1016/j.dsr.2022.103955, 2023.

Meister, P., Wiedling, J., Lott, C., Bach, W., Kuhfuß, H., Wegener, G., Böttcher, M. E., Deusner, C., Lichtschlag, A., Bernasconi, S. M., and Weber, M.: Anaerobic methane oxidation inducing carbonate precipitation at abiogenic methane seeps in the Tuscan archipelago (Italy), PLoS ONE, 13, e0207305, https://doi.org/10.1371/journal.pone.0207305, 2018.

Meyers, P. A.: Preservation of elemental and isotopic source identification of sedimentary organic matter, Chem. Geol., 114, 289–302, https://doi.org/10.1016/0009-2541(94)90059-0, 1994.

Niemann, H., and Elvert, M.: Diagnostic lipid biomarker and stable carbon isotope signatures of microbial communities mediating the anaerobic oxidation of methane with sulphate, Org. Geochem., 39, 1668–1677, https://doi.org/10.1016/j.orggeochem.2007.11.003, 2008.

Nowicka, B., and Kruk, J.: Occurrence, biosynthesis and function of isoprenoid quinones, Biochim. Biophys. Acta Bioenerg., 1797, 1587–1605, https://doi.org/10.1016/j.bbabio.2010.06.007, 2010.

Park, B.-J., Park, S.-J., Yoon, D.-N., Schouten, S., Sinninghe Damsté, J. S., and Rhee, S.-K.: Cultivation of autotrophic ammonia-oxidizing archaea from marine sediments in coculture with sulfur-oxidizing bacteria, Appl. Environ. Microbiol., 76, 7575–7587, https://doi.org/10.1128/AEM.01478-10, 2010.

Park, S.-J., Ghai, R., Martín-Cuadrado, A.-B., Rodríguez-Valera, F., Chung, W.-H., Kwon, K., Lee, J.-H., Madsen, E. L., and Rhee, S.-K.: Genomes of two new ammonia-oxidizing archaea enriched from deep marine sediments, PLoS ONE, 9, e96449, https://doi.org/10.1371/journal.pone.0096449, 2014.

Redshaw, E., Oueslati, G., Umoh, U. U., MacAdam, N., Granados, P., Bentley, J. N., Ahangarian, N., Bennett, R., Baghalabadi, V., Fowler, M. G., MacDonald, A., Hubert, C. R. J., and Ventura, G. T.: Microbial and geochemical architecture of an active Scotian Slope cold seep, Front. Microbiol., 17, 1709097, https://doi.org/10.3389/fmicb.2026.1709097, 2026.

Ren, Z., Wang, M., Yu, J., Zhang, L., Lin, Z., Li, X., and Zhang, Y.: Unearthing vertical stratified archaeal community and associated methane metabolism in thermokarst sediments, Environ. Microbiol., 27, e70110, https://doi.org/10.1111/1462-2920.70110, 2025.

Ruff, S. E., Biddle, J. F., Teske, A. P., Knittel, K., Boetius, A., and Ramette, A.: Global dispersion and local diversification of the methane seep microbiome, Proc. Natl. Acad. Sci. USA, 112, 4015–4020, https://doi.org/10.1073/pnas.1421865112, 2015.

Sherwin, D. F.: Scotian Shelf and Grand Banks, in The Future Petroleum Provinces of Canada: Their Geology and Potential, McCrossan, R. G. (Ed.), Canadian Society of Petroleum Geologists, Memoir 1, 519–559, 1973.

Song, J., Hwang, J., Kang, I., and Cho, J.-C.: A sulfate-reducing bacterial genus, Desulfosediminicola gen. nov., comprising two novel species cultivated from tidal-flat sediments, Sci. Rep., 11, 19978, https://doi.org/10.1038/s41598-021-99469-5, 2021.

Sintes, E., De Corte, D., Haberleitner, E., and Herndl, G. J.: Geographic distribution of archaeal ammonia oxidizing ecotypes in the Atlantic Ocean, Front. Microbiol., 7, 77, https://doi.org/10.3389/fmicb.2016.00077, 2016.

Stüeken, E. E., Long, A., Rochelle-Bates, N., and Teske, A.: Deep-marine brine seeps stimulate microbial nitrogen cycling: implications for the formation of sediment-hosted ore deposits, J. Geophys. Res. Biogeosci., 129, e2024JG008189, https://doi.org/10.1029/2024JG008189, 2024.

https://doi.org/10.5194/egusphere-2026-5038
Preprint. Discussion started: 25 August 2026

Sturt, H. F., Summons, R. E., Smith, K., Elvert, M., and Hinrichs, K.: Intact polar membrane lipids in prokaryotes and sediments deciphered by high-performance liquid chromatography/electro spray ionization multistage mass spectrometry– new biomark ers for biogeochemistry and microbial ecology, Rap. Comm. MassSpectrom., 18, 617–628, https://doi.org/10.1002/rcm.1378, 2004.

Suess, E.: Marine cold seeps and their manifestations: geological control, biogeochemical criteria and environmental conditions, Int. J. Earth Sci., 103, 1889–1916, https://doi.org/10.1007/s00531-014-1016-0, 2014.

Sun, M.-Y., Lee, C., and Aller, R. C.: Laboratory studies of oxic and anoxic degradation of chlorophyll-a in Long Island Sound sediments, Geochim. Cosmochim. Acta, 57, 147–157, https://doi.org/10.1016/0016-7037(93)90475-C, 1993.

Suzuki, D., Ueki, A., Amaishi, A., and Ueki, K.: Desulfoluna butyratoxydans gen. nov., sp. nov., a novel Gram-negative, butyrate-oxidizing, sulfate-reducing bacterium isolated from an estuarine sediment in Japan, Int. J. Syst. Evol. Microbiol., 58, 826–832, https://doi.org/10.1099/ijs.0.65306-0, 2008.

Szymczak-Żyła, M., Kowalewska, G., and Louda, J. W.: Chlorophyll-a and derivatives in recent sediments as indicators of productivity and depositional conditions, Mar. Chem., 125, 39–48, https://doi.org/10.1016/j.marchem.2011.02.002, 2011.

Treude, T., Niggemann, J., Kallmeyer, J., Wintersteller, P., Schubert, C. J., Boetius, A., and Jørgensen, B. B.: Anaerobic oxidation of methane and sulfate reduction along the Chilean continental margin, Geochim. Cosmochim. Acta, 69, 2767–2779, https://doi.org/10.1016/j.gca.2005.01.002, 2005.

Urakawa, H., Yoshida, T., Nishimura, M., and Ohwada, K.: Characterization of depth-related changes and site-specific differences of microbial communities in marine sediments using quinone profiles, Fish. Sci., 71, 174–182, https://doi.org/10.1111/j.1444-2906.2005.00945.x, 2005.

Van Mooy, B. A. S., and Fredricks, H. F.: Bacterial and eukaryotic intact polar lipids in the eastern subtropical South Pacific: water-column distribution, planktonic sources, and fatty acid composition, Geochim. Cosmochim. Acta, 74, 6499–6516, https://doi.org/10.1016/j.gca.2010.08.026, 2010.

Vernet, M., and Lorenzen, C. J.: The relative abundance of pheophorbide a and pheophytin a in temperate marine waters, Limnol. Oceanogr., 32, 352–358, https://doi.org/10.4319/lo.1987.32.2.0352, 1987.

Wade, J. A. and MacLean, B. C.: The geology of the Southeastern Margin of Canada, Chapter 5, in: Geology of the Continental Margin of Eastern Canada, edited by: Keen, M. J. and Williams, G. L., Geological Survey of Canada, The Geology of Canada, 190–238, https://doi.org/10.1130/DNAG-GNA-I1.167, 1990.

Wakeham, S.: Diagenesis of organic matter at the water-sediment interface, in: Chemistry of Marine Water and Sediments, Gianguzza, A., Pelizzetti, E., and Sammartano, S. (Eds.), Springer, Berlin, Heidelberg, 147–164, https://doi.org/10.1007/978-3-662-04935-8_6, 2002.

Wang, X., Zhao, D., Yu, T., Zhu, Y., Jiang, M., Liu, Y., Hu, S., Luo, Y., Xiang, H., and Zheng, Y.: Biological nitrogen fixation driven by methane anaerobic oxidation supports the complex biological communities in cold-seep habitat, Environ. Technol. Innov., 37, 103938, https://doi.org/10.1016/j.eti.2024.103938, 2025.

Whiticar, M. J.: Carbon and hydrogen isotope systematics of bacterial formation and oxidation of methane, Chem. Geol., 161, 291–314, https://doi.org/10.1016/S0009-2541(99)00092-3, 1999.

Wörmer, L., Lipp, J. S., and Hinrichs, K.-U.: Comprehensive Anal ysis of Microbial Lipids in Environmental Samples Through HPLC-MS Protocols, in: Hydrocarbon and Lipid Microbiology Protocols, edited by: McGenity, T. J., Timmis, K. N., and No gales, B., Springer Berlin Heidelberg, Berlin, Heidelberg, 289 317, https://doi.org/10.1007/8623_2015_183, 2015.

Wernand, M. R., van der Woerd, H. J., and Gieskes, W. W. C.: Trends in ocean colour and chlorophyll concentration from 1889 to 2000, worldwide, PLoS ONE, 8, e63766, https://doi.org/10.1371/journal.pone.0063766, 2013.

Xue, Y., Lu, H., Li, Y., Yang, H., Tang, Y., and Lu, Y.: Anaerobic oxidation of methane by manganese oxides in marine sediments: a review, Front. Mar. Sci., 12, 1609892, https://doi.org/10.3389/fmars.2025.1609892, 2025.

https://doi.org/10.5194/egusphere-2026-5038
Preprint. Discussion started: 25 August 2026

Yoshinaga, M. Y., Kellermann, M. Y., Rossel, P. E., Schubotz, F., Lipp, J. S., and Hinrichs, K.: Systematic fragmentation patterns of archaeal intact polar lipids by high-performance liquid chromatography/electrospray ionization ion-trap mass spectrometry, Rap. Comm. Mass Spectrom., 25, 3563–3574, https://doi.org/10.1002/rcm.5251, 2011.

Zeng, T., Liu, C., Yang, Q., Zhao, J., and Ji, F.: Distribution and variation characteristics of branched glycerol dialkyl glycerol tetraethers (brGDGTs) in sediment cores along the nearshore-to-offshore gradient of the East China Sea and their correlation with microbial community diversity, Biology, 14, 1077, https://doi.org/10.3390/biology14081077, 2025.

Zhang, T., He, W., Liang, Q., Zheng, F., Xiao, X., Zeng, Z., Zhou, J., Yao, W., Chen, H., Zhu, Y., Zhao, J., Zheng, Y., and Zhang, C.: Lipidomic diversity and proxy implications of archaea from cold seep sediments of the South China Sea, Front. Microbiol., 14, 1241958, https://doi.org/10.3389/fmicb.2023.1241958, 2023.

Zhang, Y. G., Zhang, C. L., Liu, X.-L., Li, L., Hinrichs, K. U., and Noakes, J. E.: Methane Index: A tetraether archaeal lipid biomarker indicator for detecting the instability of ma rine gas hydrates, Earth. Planet. Sci. Lett., 307, 525–534, https://doi.org/10.1016/j.epsl.2011.05.031, 2011.

Zhao, Y., Liu, Y., Cao, S., Hao, Q., Liu, C., and Li, Y.: Anaerobic oxidation of methane driven by different electron acceptors: a review, Sci. Total Environ., 946, 174287, https://doi.org/10.1016/j.scitotenv.2024.174287, 2024.

Zhang, Z.-X., Li, J., Chen, Z., Sun, Z., Yang, H., Fu, M., and Peng, X.: The effect of methane seeps on the bacterial tetraether lipid distributions at the Okinawa Trough, Mar. Chem., 225, 103845, https://doi.org/10.1016/j.marchem.2020.103845, 2020.

Zhang, Z.-X., Li, J., Lu, H., Yang, H., Zhang, Y., Tang, Y., et al.: Bacterial glycerol tetraethers as a potential tool to trace marine methane cycling, Limnol. Oceanogr., 69, 104–120, https://doi.org/10.1002/lno.12462, 2024.